JGR Space Physics

RESEARCH ARTICLE
10.1029/2022JA030939

**Key Points:**

- Delay of the release of in situ electrons from hard X-ray generating electrons in impulsive solar energetic particle events is examined for 29 events
- Clear delays are seen in all events and in most events the delay is energy dependent
- The delay shows no energy dependence in fewer than 20% events and the traditional velocity dispersion analysis method only applies in these events

**Correspondence to:**
G. Li,
gangli.uahuntsville@gmail.com

**Citation:**
Wu, X., Li, G., Zhao, L., Effenberger, F., Wang, L., & Yao, S. (2023). Statistical study of release time and its energy dependence of in situ energetic electrons in impulsive solar flares. *Journal of Geophysical Research: Space Physics*, *128*, e2022JA030939. https://doi.org/10.1029/2022JA030939

Received 17 AUG 2022
Accepted 23 FEB 2023



# Statistical Study of Release Time and Its Energy Dependence of In Situ Energetic Electrons in Impulsive Solar Flares

**Xiangyu Wu[1,2], Gang Li[2], Lulu Zhao[3], Frederic Effenberger[4,5], Linghua Wang[6], and Shuo Yao[1]**

[1]School of Geophysics and Information Technology, China University of Geosciences, Beijing, China, [2]Department of Space Sciences, University of Alabama in Huntsville, Huntsville, AL, USA, [3]Department of Climate and Space Sciences and Engineering (CLaSP), University of Michigan, Ann Arbor, MI, USA, [4]Institut für Theoretische Physik, IV, Ruhr-Universität Bochum, Bochum, Germany, [5]Bay Area Environmental Research Institute, NASA Research Park, Moffett Field, CA, USA, [6]School of Earth and Space Sciences, Peking University, Beijing, People's Republic of China

**Abstract** Using the fraction velocity dispersion analysis method, it has been shown recently that in two impulsive solar energetic electron (SEE) events, the release times of near-relativistic electrons at the Sun for outward-propagating electrons are energy dependent and are delayed compared to those of the downward-propagating electrons. In this work, we perform a statistical study of the release time and its energy dependence of near-relativistic electrons in impulsive SEE events. We use in situ observations from the WIND spacecraft and remote hard X-ray observations from the RHESSI and/or Fermi spacecraft. The difference in the release times between outward electrons and downward electrons for 29 events is obtained. In all events, the release of the outward-propagating electrons is delayed from those precipitating downward. In 26 of the 29 events, the release times of outward-propagating electrons also show clear energy dependence. In 15 of these 26 events, in situ electron data from more than five energy channels were available. The delay time as a function of energy for nine of these can be fitted by a form proposed by G. Li et al. (2021, https://doi.org/10.1029/2021GL095138). The implication of this energy-dependent release on the Magnetohydrodynamics turbulence property at the electron acceleration site is discussed.

## 1. Introduction

While solar flares are generally regarded as a major site that accelerates solar energetic particles (SEPs), the underlying acceleration mechanism is still under debate. In the standard flare model (CSHKP model; Carmichael, 1964; Hirayama, 1974; Kopp & Pneuman, 1976; Sturrock, 1966), ions and electrons are accelerated by the released magnetic energy during magnetic reconnection. Electrons precipitating to the solar surface generate hard X-ray (HXR), and due to the occurrence of reconnection between closed field lines, electrons cannot escape. An interchange reconnection, proposed by Heyvaerts et al. (1977), refined by Vršnak et al. (2003) and Krucker et al. (2007), introduces a scenario where magnetic reconnection occurs between closed and open field lines, leading to the escape of flare-accelerated energetic particles into the solar wind. In the work of Masson et al. (2013), an intrinsic interchange reconnection is identified to account for the escape of accelerated energetic particles into the heliosphere.

If electrons are accelerated at an interchange reconnection site, the accelerated electrons can propagate both outward and downward so that the outward-propagating electrons and the HXR-generating electrons are released at the same time, that is, simultaneous release of electrons. Recently, G. Li, Zhao, et al. (2020) and G. Li et al. (2021) tested this idea of simultaneous release in two impulsive energetic electron events, the 2001-04-25 event and the 2016-07-23 event. In both events, in situ electrons were observed by the 3D Plasma and Energetic Particle (3DP) instruments on WIND. By applying the fractional velocity dispersion analysis (FVDA) method (Zhao et al., 2019), they obtain the release times of in situ electrons at the Sun. They also used HXRs observations to obtain proxies of the release times of downward-precipitating energetic electrons. They found that in both events the outward-propagating electrons are released later than the HXR-generating electrons, indicating that these two electron populations are likely of two different populations and the simple interchange reconnection scenario cannot explain both events.

The timing study of G. Li, Zhao, et al. (2020) and G. Li et al. (2021) supports earlier results by Haggerty and Roelof (2002) and Haggerty et al. (2003) who used the Advanced Composition Explorer observations compared

to the inferred solar release time of in situ energetic electrons. For over 70 events, Haggerty and Roelof (2002) compared the release time of in situ near-relativistic electrons (using highest-energy channel available and assuming a 1.2 au nominal path length) with HXR start time and found a 10–20 min delay. In addition to a delay between the outward-propagating electrons and the downward-propagating electrons, the release of outward-propagating electrons can be also energy dependent. In the work of L. Wang et al. (2006, 2016), a delay between the injection of high-energy electrons and low-energy electrons in SEP events was found. Such a delay was also noted earlier by Krucker et al. (1999), Haggerty and Roelof (2002), Simnett et al. (2002), and Klein et al. (2005). The delay can be a natural consequence of the underlying acceleration process: it takes longer time to accelerate particles to higher energies, consequently a later release. One useful observation that can better help understand this delay is type III radio bursts. In a statistical study of 79 solar electron events, Cane (2003) examined possible delay of in situ electrons from the accompanying type III radio bursts. Using the electron release times determined by Haggerty and Roelof (2002), Cane (2003) found a correlation between this delay and solar wind density (see Figure 4 of Cane [2003]). Events with longer delays tend to have larger solar wind density. Cane (2003) suggested that interplanetary conditions such as pitch angle scattering may be responsible for such a delay and argued that type III generating electrons and in situ electrons could be of the same population. However, the uncertainty of this correlation appears to be large. Furthermore, the electron release times were determined using the traditional VDA method for selected electron energy bins (Haggerty & Roelof, 2002), which is less accurate compared to the FVDA method employed here. In this work, we also include type III radio bursts. As will be shown, there is no clear evidence of a delay between the release time of type III radio bursts and in situ electrons. Nevertheless, the work of Cane (2003) illustrated the importance of the propagation effect in examining electron events.

If indeed the delay of release is due to acceleration (other processes such as trapping may also lead to delayed releases), then the energy dependence of the delay offers an opportunity to examine the underlying acceleration process. In the 2016-07-23 event, G. Li et al. (2021) examined the energy dependence of the release times and found that the delay can be fitted by a power law form. From the power law index of the fitting, they inferred the Magnetohydrodynamics turbulence power spectrum at the acceleration site.

The work of G. Li et al. (2021) calls for a statistical study of the release time and its energy dependence of energetic electrons in impulsive events. Such a statistical study requires an accurate determination of the release times of energetic electrons at the Sun. This can be achieved by the FVDA method developed by Zhao et al. (2019). In this work, we use the FVDA method to examine the energy dependence of the release times of energetic electrons in 29 impulsive events. In all events, we find that the outward-propagating electrons are released later than those HXR-generating electrons. The release of the outward-propagating electrons shows clear energy dependence for 26 events and shows no/weak energy dependence in three events. In 15 events, in situ electron observation for more than five energy channels are obtained. For these events, we further apply the analysis in G. Li et al. (2021) to fit the energy release time delay by a power law of the electron momentum. For 9 out of 15 events, reasonable fittings were obtained and the fitting results are shown in Table 2 and Figure 5. The implication of the fitted power law index on the flare turbulence spectrum is discussed.

## 2. Event Selection and the FVDA Method

In situ energetic electrons are measured by the 3DP instrument on board the WIND spacecraft (Lin et al., 1995). The silicon semiconductor telescopes in the 3DP instrument provide three-dimensional measurements of electrons distributions from ∼25 to ∼400 keV with energy resolution of ∼7 keV Full Width at Half Maximum and angular resolution of 22.5° × 36°. Energetic electron observations are combined with the detection of type III radio bursts that are captured by WAVES instrument on board the WIND spacecraft and/or SWAVES instrument on Solar Terrestrial Relations Observatory (STEREO). HXRs are observed by either the Ramaty High Energy Solar Spectroscopic Imager (RHESSI) or the Fermi/GBM. RHESSI was launched in February 2002, and it detects solar photons from 3 keV to 17 MeV (Smith et al., 2003). Fermi was launched in June 2008, and the GBM instrument consists of 12 sodium iodide (NaI) detectors covering the energy range between 8 and 1,000 keV and two bismuth germanate (BGO) detectors covering the energies of 200 keV to 40 MeV (Meegan et al., 2009). Both RHESSI and Fermi/GBM have high time and energy resolution and are capable of determining the release time of HXR-generating electrons.

For our study, a RHESSI HXR event list and an in situ electron event list are used. The RHESSI flare list is based on the flare database maintained by the RHESSI team at https://hesperia.gsfc.nasa.gov/rhessi3/data-ac-

cess/rhessi-data/flare-list/index.html. This list is then correlated with in situ electron observations by WIND (L. Wang et al., 2012; W. Wang et al., 2021). An event is identified as a potential event if the HXR peak time from the RHESSI observation and the in situ onset time of energetic electrons from the WIND observation are within 20 min. We then select events for our study with the following criteria:

1. In situ observation of the event by WIND must have fast rising phase (onset and peak of the event must be within an hour) and the average pre-event background $+3\sigma$ should be lower than one fourth of the peak flux.
2. The time intensity profiles of in situ electrons are detected by at least four energy channels of WIND/3DP with similar shapes, in the energy range of 27–310 keV.
3. Events need to be observed by either RHESSI or Fermi in at least one of the two energy channels: 25 or 50 keV. For large solar flares with complicated magnetic field structures, HXR time profiles often show multiple peaks during the event. We take the first episode as the HXR observation of the event.

With these criteria, a total of 29 events are identified. For all these events, we do not use omni-direction electron intensity data, but only use electron data from sectors that align with the nominal Parker field direction and are sunward facing. This is to ensure that our analysis is not contaminated by possible preceding events in which inward propagating electrons may be detected during our events. Indeed, previous studies have shown evidence that energetic electrons can propagate toward the Sun due to the reflection beyond 1 au or near the Sun in a magnetic loop (Anderson et al., 1995; G. Li, Wu, et al., 2020; Tan et al., 2009, 2012). Next, we apply the FVDA method (G. Li, Zhao, et al., 2020; G. Li et al., 2021; Zhao et al., 2019) to compute the path length $L$ and the release times $T_r$ of outward-propagating electrons. In the original VDA method (Lin, 1974, 1985) and later applications of it (Laitinen et al., 2015; Lintunen & Vainio, 2004; L. Wang et al., 2011), one implicit assumption is that electron motion in the interplanetary magnetic field (IMF) can be approximated by scatter-free propagation. This is a reasonable assumption if electrons do not interact strongly with IMF turbulence and if electron mean free paths are longer than 1 au. Furthermore, as shown in the simulations by Moradi and Li (2019), when the IMF turbulence is small, electron path length is close to the field line path length. Moreover, the simulations by Moradi and Li (2019) also showed that the electron path length has little dependence on electron energy.

The basic procedure of FVDA was explained in Zhao et al. (2019). Two slightly different approaches were introduced in G. Li, Zhao, et al. (2020) and G. Li et al. (2021) in obtaining the release time $T_r$. Here, we clarify these two approaches in more detail as it is crucial for our study. These two approaches, which we name as Approach I and Approach II, will yield similar $T_r$ when electrons of different energies are released simultaneously at the Sun. When the release is energy dependent, however, Approach II should be used to obtain the release times. Whether or not the release time is energy dependent in a particular event can be judged by examining if the path length $L$ obtained from the FVDA method is physically meaningful or not (a path length shorter than 1 au would be a nonphysical path length). Below, we outline the general procedure of the FVDA with a focus on explaining the differences of the two approaches.

The steps of FVDA are the following: for each energy channel $E_i$, we identify from the electron time intensity profile a time $t_i(\eta)$ that corresponds to an intensity that is a fraction $\eta$ of the peak intensity. For each $\eta$, we then apply the VDA to obtain a release time $T_r(\eta)$ and a path length $L(\eta)$ which are now functions of $\eta$. Assuming electrons of different energies are released simultaneously at the Sun, one can now take $\eta \to 0$ and obtain $T_r(\eta \to 0)$ and $L(\eta \to 0)$ which represent estimates of the release time and path length. Comparing to the VDA, the FVDA makes use of the entire rising phase of the electron time intensity profile and the procedure of taking $\eta \to 0$ provides a self-consistent check and uncertainty measure for the resulting $T_r$ and $L$.

In obtaining the release time of electrons, two approaches can be used. In Approach I, we consider $T_r(\eta)$ as a function of $\eta$ and take the limit of $\eta \to 0$ directly to obtain $T_r(\eta \to 0)$. In Approach II, one first obtains the onset time $t_i$ (for electron in the $i$th energy bin) from the time intensity profile by taking $\eta \to 0$ and then obtains the corresponding release times at the Sun. To implement this approach, we approximate the $t_i(\eta)$ as a polynomial in $\eta$,

$$t_i(\eta) = a\eta^2 + b\eta + t_i^0 \tag{1}$$

where $t_i^0$ is the onset time of the $i$th energy channel (corresponding to $\eta = 0$). Using multiple $(\eta, t(\eta))$ pairs, we can fit the parameters $a$, $b$, and $t_i^0$. Once the onset time is obtained, one can compute the release time $T_r$ of electrons at the Sun from

$$T_r(E_i) = t_i^0 - L/(\beta_i c) \tag{2}$$

where $E_i$ is the energy of the $i$th bin (using median value), $\beta_i c$ is the speed of electron in $i$th bin, and $L$ is an assumed path length. Note that $L$ can be taken as $L(\eta)$ from the fitting and with $\eta \to 0$) but does not need to be. In fact, as shown in Zhao et al. (2019), $L(\eta \to 0)$ can be smaller than 1 au in many events. Such a nonphysical value is a direct consequence of (incorrectly) assuming that electrons of different energies are released simultaneously at the Sun. Clearly when $L(\eta \to 0) < 1$ au, we should use Approach II and use a more physical value of $L$ in Equation 2. Approach II of the FVDA method allows one to infer an energy-dependent release and obtain the corresponding energy-dependent release times of energetic electrons at the Sun. As pointed out in G. Li et al. (2021), this was not possible in the traditional VDA method since electrons of all energies are assumed to be released at the Sun simultaneously in the VDA.

A reasonable value of $L$ to be used in Equation 2 is the nominal Parker path length, which depends on the solar wind speed. Note that foot point random walk can lead to meandering field lines and affect the field line path length. However, the work by Moradi and Li (2019) and Bian and Li (2022) suggested that in the case of solar wind, the path length of meandering field line does not differ much from the nominal Parker value. In this study, we consider three different values of $L$ in Equation 2 when using Approach II (see discussion below).

Note that for the cases with simultaneous release (i.e., release is energy independent), $T_r$ from Approach I and Approach II should be close if the meandering field line does not deviate much from the Parker field. Among the 29 events we examine in this work, 3 events have energy-independent release times of in situ electrons at the Sun. In these three events, as expected, the release times from Approach I are found to be close to those obtained from Approach II and both close to the Parker field path length. This agreement provides a self-consistent check for our analysis.

Figure 1 shows the results of FVDA for four events which occurred on 2005-05-16, 2002-08-20, 2003-01-13, and 2004-10-04, respectively. Using Approach II, the deduced $T_r$ of in situ electrons at the Sun are shown as blue, orange, and green circles for three different choices of the path length. The blue circles are for a path length from using Approach I of FVDA. If the calculated $L$ is smaller than 1 au, we set it to 1 au. The orange circles assume a path length given by a nominal Parker spiral field using an average solar wind speed from a 12-hr window prior to the event. The green circles correspond to a complementary choice of path length to the blue and orange symbols. It is chosen such that it is longer (shorter) than the Parker path length if the blue symbol corresponds to a path length shorter (longer) than the Parker length; and the arithmetic average between the path lengths for the green and the blue symbols is the Parker path length. HXR start times at the Sun are marked by red stars. The insets inside each panel are the FVDA analyses for $\eta = 0.35$, 0.2, 0.06, and 0 using Approach I. These are labeled as solid "triangle," "square," "circle," and "diamond," respectively. In Figure 1a, the release times of outward-propagating electrons show a clear energy dependence, with electrons of higher energy released at a later time. This is consistent with the fact that the path length from Approach I is shorter than 1 au. For events in panels (b)–(d), the release times of outward electrons show little energy dependence. Indeed, using $L = L_{\text{Parker}}$ (corresponding to the orange symbols) $T_r$s for electrons of different energies are within 1 min in all three events. Using the other two choices of the path length (green and blue symbols) still lead to energy-independent release times. Moreover, the path lengths from Approach I in these three events are very close to the corresponding Parker field path lengths, indicating that the results from Approach I and Approach II are similar. Note that in situ electron data from the Wind/3DP have a very refined time resolution of 12 s. In applying FVDA, we also apply the Savitzky-Golay filter with a window size of ∼7 data points. For some events, the data count for the 181 and 310 keV energy channels is low and a window size of ∼11 s is used. Compared to the well-known boxcar averaging, the Savitzky-Golay filter estimates the sample value at the center of a window using a polynomial fitting (Baba et al., 2014; Savitzky & Golay, 1964). This helps to improve the signal-to-noise ratio of the data while preserving the position and width of the peaks, which is beneficial for our timing study. The Savitzky-Golay filter technique has been practiced in solar/heliospheric science before, see for example, Williams and Pesnell (2011) and Mitchell et al. (2020). Although the filter itself does not change the time resolution, it introduces a source of uncertainty in determining $t(\eta)$ and therefore the release time. We assume the uncertainty of $t(\eta)$ is 2.5 times the time resolution, which is 30 s in this work. Note that because the rising phase of the time intensity profile is very rapid, a change of $t(\eta)$ by 30 s often leads to a large change of $\eta$, suggesting that the uncertainty of $t(\eta)$ is likely smaller than 30 s.

In this work, to judge if the outward-propagating electrons are released simultaneously at the Sun, we use a 1-min threshold. If the release time difference between any two energy channels in a given event is shorter than 1 min, then

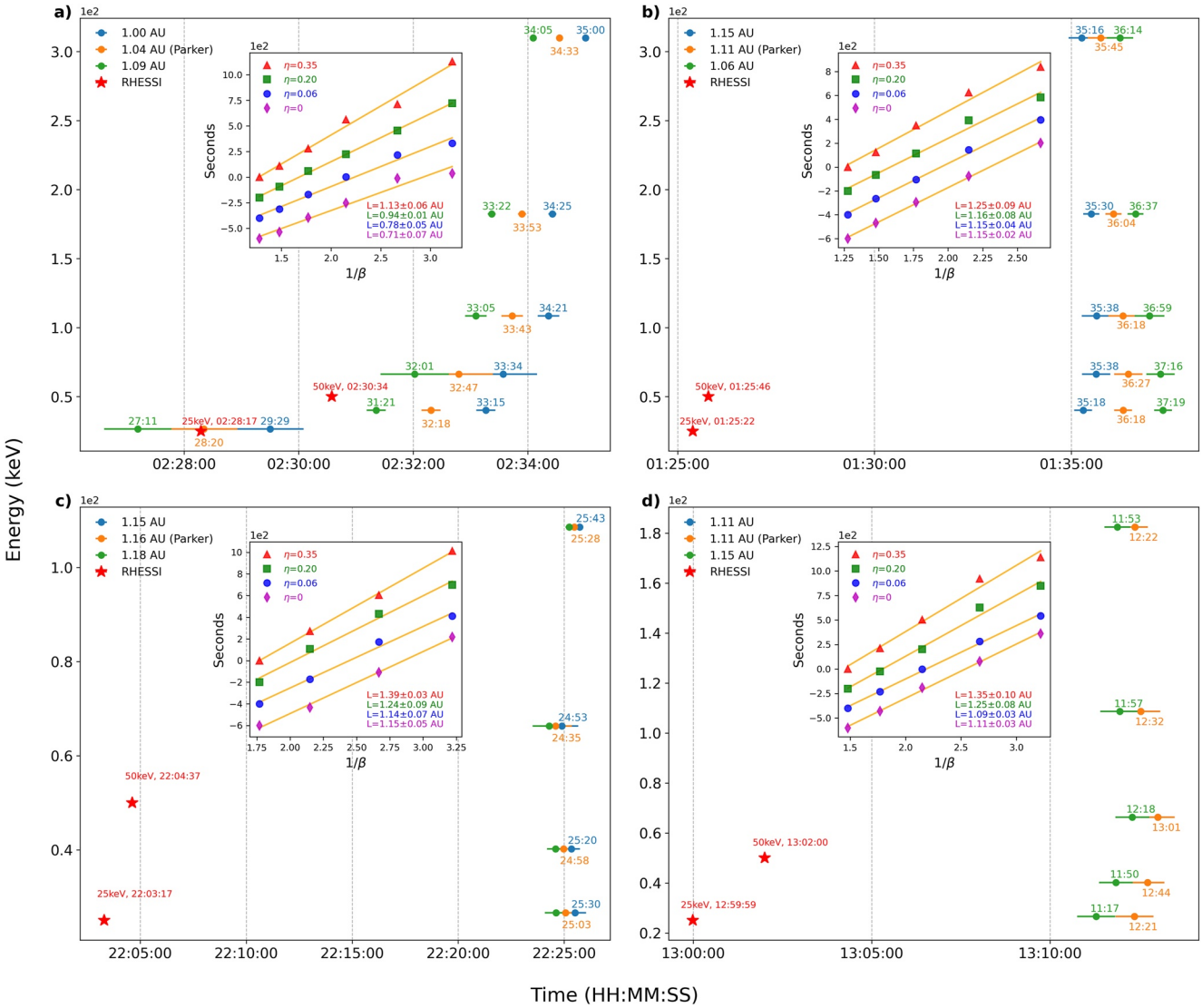


**Figure 1.** Electron release times as a function of energy for four example events. In all panels, the *y*-axis is electron energy, the *x*-axis is time. The green, orange, and blue symbols correspond to three different path lengths used in Equation 2 when using Approach II of fraction velocity dispersion analysis (FVDA). The red stars mark the start times of hard X-rays at the Sun. The insets in each panel show the FVDA plots for four different $\eta$s: 0.35, 0.20, 0.06, and 0 using Approach I of FVDA. See text for details.

that event is classified as an energy-independent release event; otherwise it is classified as an energy-dependent release event. With this criterion, three events are found to be energy-independent release events. They are shown in Figures 1b–1d. If we relax the threshold from 1 to 2 min, the number of energy-independent release events will increase to 5, which we will discuss in Section 3.3. Note that the occurrence rate of energy-independent release is low, only 3/29 ∼ 10% if using a 1-min threshold, and 5/29 ∼ 17% if using a 2-min threshold. Therefore using the traditional VDA analysis in impulsive events would be inappropriate, and FVDA should be used.

## 3. Results and Discussion

As discussed in the last section, a total of 29 events were identified in our study. These events are listed in Table 1. Columns 1 and 2 are the event number and date of the events. Columns 3–6 contain the HXR onset/peak times observed by RHESSI at the 12–25 and 25–50 keV energy channels. Note that the HXR times are the observed time at 1 au and have not been corrected for the travel time. As in G. Li, Zhao, et al. (2020), we use the HXR energy as a proxy for that of the parent electrons. The intensity profile of the HXR is the energy-integrated solar

Journal of Geophysical Research: Space Physics
10.1029/2022JA030939

**Table 1**
*Event List*

| Id | Date | HXR 12–25 keV Onset | HXR 12–25 keV Peak | HXR 25–50 keV Onset | HXR 25–50 keV Peak | Type III[a] | $T_r$ of electrons (keV) 26.6 | 40.2 | 66.3 | 108.6 | 182.4 | 310 | Path length Parker | Path length FVDA | Class | AR | Note |
|---|---|---|---|---|---|---|---|---|---|---|---|---|---|---|---|---|---|
| 1 | 2002-05-06 | 23:42:58 | 23:56:56 | 23:55:31 | 23:56:56 | 23:43:33 | 23:51:06 | 23:52:46 | 23:53:56 | 23:53:03 | | | 1.17 | 0.99 ± 0.092 | C6.4 | | |
| 2 | 2002-07-18 | 23:12:17 | 23:15:12 | 23:13:05 | 23:15:12 | 23:54:30 | 23:54:32 | 23:55:01 | 23:55:37 | 23:56:26 | | | 1.17 | 1.02 ± 0.022 | C8.2 | | |
| 3 | 2002-08-20 | 01:33:42 | 01:40:20 | 01:34:06 | 01:40:16 | 01:30:39 | | 01:36:19 | 01:36:27 | 01:36:19 | 01:36:04 | 01:35:45 | 1.11 | 1.15 ± 0.022 | M5.0 | 10069 | [b] |
| 4 | 2002-08-20 | 08:24:36 | 08:26:00 | 08:24:44 | 08:25:36 | 08:16:36 | | 08:28:33 | 08:28:35 | 08:28:40 | 08:27:59 | 08:27:46 | 1.11 | 1.18 ± 0.033 | M3.4 | 10069 | |
| 5 | 2003-01-13 | 22:11:37 | 22:15:40 | 22:12:56 | 22:15:44 | 22:13:50 | 22:25:04 | 22:24:58 | 22:24:35 | 22:25:29 | | | 1.16 | 1.15 ± 0.048 | C2.1 | | [b] |
| 6 | 2003-07-08 | 02:17:16 | 02:17:48 | | | 02:17:39 | 02:16:21 | 02:17:45 | 02:18:27 | 02:20:47 | | | 1.10 | 0.76 ± 0.072 | C2.3 | 10397 | |
| 7 | 2003-07-09 | 16:26:44 | 16:31:48 | | | 16:17:55 | 16:46:41 | 16:52:04 | 16:55:35 | 17:00:03 | | | 1.14 | 0.07 ± 0.070 | C5.8 | 10397 | |
| 8 | 2003-10-04 | 13:08:18 | 13:14:40 | 13:10:19 | 13:16:40 | 13:14:45 | 13:12:22 | 13:12:44 | 13:13:01 | 13:12:33 | 13:12:23 | | 1.11 | 1.11 ± 0.027 | C2.5 | | [b] |
| 9 | 2004-02-28 | 03:18:16 | 03:19:08 | 03:18:05 | 03:18:24 | 03:10:53 | 03:12:25 | 03:15:11 | 03:17:20 | 03:18:31 | 03:18:44 | | 1.18 | 0.73 ± 0.048 | B6.6 | 10564 | |
| 10 | 2004-07-24 | 18:22:52 | 18:26:44 | | | 18:36:31 | 18:36:51 | 18:38:13 | 18:38:04 | 18:39:19 | | | 1.08 | 0.90 ± 0.054 | C1.1 | 10652 | |
| 11 | 2004-11-01 | 03:17:36 | 03:20:08 | 03:17:45 | 03:19:00 | 03:09:53 | 03:19:20 | 03:21:13 | 03:21:15 | 03:20:17 | 03:21:37 | | 1.13 | 1.03 ± 0.070 | M1.1 | 10691 | |
| 12 | 2005-05-16 | 02:36:36 | 02:41:28 | 02:38:53 | 02:40:16 | 02:31:41 | 02:28:21 | 02:32:19 | 02:32:48 | 02:33:44 | 02:33:54 | 02:34:33 | 1.04 | 0.71 ± 0.067 | M1.4 | 10763 | |
| 13 | 2005-09-04 | 15:10:25 | 15:11:52 | 15:10:23 | 15:13:44 | | | 15:00:09 | 15:02:09 | 15:02:16 | 15:02:10 | | 1.06 | 0.85 ± 0.090 | C2.0 | 10803 | [c] |
| 14 | 2006-11-19 | 22:54:23 | 23:02:40 | 22:52:13 | 23:03:48 | 22:51:46 | 22:48:26 | 22:50:14 | 22:49:09 | 22:50:30 | 22:52:44 | | 1.16 | 0.93 ± 0.096 | | | |
| 15 | 2006-11-20 | 03:34:10 | 03:35:36 | | | 03:26:49 | | 03:24:44 | 03:27:05 | 03:28:05 | 03:29:07 | | 1.17 | 0.73 ± 0.034 | | | |
| 16 | 2006-11-21 | 08:28:52 | 08:29:16 | | | 08:20:53 | | 08:19:49 | 08:20:27 | 08:21:08 | 08:22:33 | | 1.21 | 0.95 ± 0.062 | B2.3 | | |
| 17 | 2006-11-21 | 16:17:14 | 16:20:12 | | | 16:41:44 | 16:40:26 | 16:41:55 | 16:42:36 | 16:44:43 | | | 1.20 | 0.87 ± 0.061 | B3.3 | | |
| 18 | 2011-05-15 | 23:28:23 | 23:31:02 | 23:29:24 | 23:31:02 | 23:20:39 | 23:22:14 | 23:25:55 | 23:28:19 | 23:29:12 | 23:29:03 | | 1.10 | 0.61 ± 0.087 | C4.8 | 11208 | |
| 19 | 2011-07-31 | 19:03:58 | 19:06:28 | 19:04:42 | 19:04:44 | 18:57:04 | 18:59:44 | 19:00:44 | 19:02:46 | 19:03:26 | | | 1.07 | 0.74 ± 0.037 | C1.7 | 11265 | |
| 20 | 2011-08-08 | 15:31:55 | 15:35:09 | 15:34:02 | 15:35:05 | 15:51:00 | 15:52:30 | 15:55:21 | 15:55:50 | 15:57:49 | | | 1.09 | 0.69 ± 0.075 | B8.1 | 11263 | |

Journal of Geophysical Research: Space Physics

10.1029/2022JA030939

**Table 1**
*Continued*

| Id | Date | HXR 12–25 keV | | HXR 25–50 keV | | Type III[a] | $T_r$ of electrons (keV) | | | | | | Path length | | Class | AR | Note |
|---|---|---|---|---|---|---|---|---|---|---|---|---|---|---|---|---|---|
| | | Onset | Peak | Onset | Peak | | 26.6 | 40.2 | 66.3 | 108.6 | 182.4 | 310 | Parker | FVDA | | | |
| 21 | 2011-08-09 | 08:00:23 | 08:04:04 | 08:00:34 | 08:03:44 | 07:54:39 | 07:54:23 | 07:56:56 | 07:59:11 | 07:59:52 | 08:00:13 | 08:00:13 | 1.07 | 0.71 ± 0.051 | X6.9 | 11263 | |
| 22 | 2012-09-27 | 23:47:14 | 23:48:06 | 23:47:26 | 23:48:06 | 00:06:46 | | 00:09:35 | 00:06:41 | 00:07:37 | 00:05:18 | 00:05:16 | 1.15 | 1.51 ± 0.097 | C3.7 | 11577 | |
| 23 | 2013-11-13 | 10:30:26 | 10:31:52 | 10:30:46 | 10:31:48 | 10:22:52 | 10:36:35 | 10:37:31 | 10:38:46 | 10:40:26 | | | 1.16 | 0.85 ± 0.046 | C3.5 | 11890 | |
| 24 | 2014-02-20 | 07:40:00 | 07:49:08 | 07:40:53 | 07:45:20 | 07:40:03 | 07:39:49 | 07:43:40 | 07:45:49 | 07:46:50 | 07:47:10 | | 1.10 | 0.59 ± 0.075 | M3.0 | 11976 | |
| 25 | 2014-03-28 | 23:45:13 | 23:49:35 | 23:48:15 | 23:49:07 | 23:39:34 | 23:46:00 | 23:47:53 | 23:49:25 | 23:50:07 | 23:50:06 | | 1.14 | 0.85 ± 0.041 | M2.6 | 12017 | |
| 26 | 2014-06-12 | 10:48:42 | 10:49:13 | 10:48:46 | 10:49:13 | 10:48:44 | 10:49:15 | 10:49:54 | 10:50:44 | 10:50:04 | | | 1.10 | 1.02 ± 0.054 | M2.7 | 12085 | |
| 27 | 2014-06-12 | 13:10:49 | 13:14:32 | | | 13:13:40 | 13:13:40 | 13:15:30 | 13:16:10 | 13:17:02 | 13:17:32 | 13:17:46 | 1.11 | 0.86 ± 0.020 | C3.8 | 12080 | |
| 28 | 2016-07-20 | 22:03:32 | 22:11:52 | 22:05:01 | 22:06:52 | 21:56:27 | 21:54:37 | 21:57:17 | 21:58:35 | 21:58:55 | 21:59:30 | 21:59:57 | 1.10 | 0.79 ± 0.040 | C4.6 | 12567 | |
| 29 | 2016-07-23 | 05:06:32 | 05:15:00 | 05:09:07 | 05:10:40 | 05:02:04 | 05:02:15 | 05:05:03 | 05:06:58 | 05:07:44 | 05:08:42 | 05:09:13 | 1.14 | 0.74 ± 0.030 | M7.6 | 12567 | |

[a]The propagation time has been subtracted from the time of type III radio bursts. [b]Energy-independent release of in situ electrons. [c]The HXR onset times can be delayed from the real values due to data gap.

atmosphere response to the precipitating energetic electrons. To obtain the onset time of HXR, we first identify a background period (~5–10 min) before the event, then for each energy channel, the onset time of HXR is obtained as the time when the photon intensity is $3\sigma$ above the background. We use this time as the estimate for the release time of downward-propagating electrons. Column 7 contains times of type III radio bursts near the Sun. The times have been corrected for the travel time based on the location of the spacecraft, and they are to be compared with the release times of the in situ electrons at the Sun. Columns 8–13 contain the release times of electrons for six energy channels from 26.6 to 310 keV at the Sun using Approach II and assuming a path length corresponding to the nominal Parker field, as shown in column 14. Column 15 is the path length obtained from Approach I. Column 16 is the flare class of the event. Column 17 is the NOAA designated active region (AR) numbers of the flare events. This information is obtained from the Heliophysics Event Knowledgebase (HEK) through SUNPY *hek* module https://docs.sunpy.org/en/stable/guide/acquiring_data/hek.html. If no data is available for a given event, this field is left blank.

Solar energetic electron (SEE) events are often accompanied by type III radio bursts (L. Wang et al., 2012). Since the propagation of radio waves in the solar wind is not affected by the IMF, type III radio bursts can provide valuable information on electron release times. However, a one-to-one association between type III radio bursts and in situ electron events can be subject to large uncertainty due to the following. First, a single solar eruption may consist of multiple type III radio bursts, leading to ambiguity in the association between type III radio bursts and in situ electrons. Second, the generation of type III radio bursts depends on many factors, and not all energetic electron beams may generate type III radio bursts (Cairns et al., 2018). In our work, of all 29 events, event 13 had no type III radio bursts observation. This is possible if the electron streams did not excite radio waves (Cairns et al., 2018). For the rest 28 events, 11 events: 1, 2, 4, 7, 12, 16, 18, 21, 23, 24, and 28 had only single type III radio bursts, so the identification of type III bursts in these events was unambiguous. The remaining 17 events have multiple type III radio bursts associated and we identify the type III burst as the one whose release time is closest to the release time of the lowest energy in situ electrons. With this choice, from Table 1 we can see that the release times of the outward-propagating electrons from our FVDA are consistent with the type III release times in 15 of 28 events. In these events, the time differences between the onset time of type III bursts and electron release time are within 1 min, suggesting that the type III radio-burst-generating electrons and the in situ electrons are of the same population. These are events 2, 6, 10, 12, 15–17, 20–22, 24, and 26–29. Note that previous studies (Haggerty & Roelof, 2002; Krucker et al., 1999) have found that only a small percentage of the events they studied showed no delay between the inferred release times of the in situ electrons and the type III radio bursts. However, in these studies, the release times of in situ electrons are obtained from the traditional VDA method, which, as pointed out by Zhao et al. (2019), is subject to large uncertainties since the onset time of in situ electrons can be hard to obtain. Here, using FVDA, we found that the type III radio bursts (or one episode of multiple bursts) in more than half events coincide with the release of in situ electrons. For the rest 13 events, except events 8 and 14, the release times of type III radio bursts are earlier than the release times of in situ electrons. It is possible that in these events the type III radio bursts are excited by other streams of energetic electrons. Incidentally, we note that in events 1, 3, 9, 18, 19, and 25, the onset times of type III radio bursts are within 8-min of the electron release time. An 8-min window has been identified by L. Wang et al. (2006) who found the injection time of electrons at 13–300 keV was $7.6 \pm 1.3$ min later than the type III radio bursts in impulsive electron events. In the rest five events (events 4, 5, 7, 11, and 23), the type III bursts precede the in situ electrons by more than 10 min.

It is interesting to note that for the 11 events where type III radio bursts precede the release of in situ electrons, seven events, events 4, 7, 9, 11, 18, 23, and 25, have the release times of type III radio bursts consistent (within 1 min) with the release time of HXRs. Without observations of in situ electrons, this observation may suggest that the HXR-generating electrons and the type III radio-bursts-generating electrons are of the same population. However, note that type III radio burst is only a proxy of low-energy (10–20 keV) electrons, and, as one can see from Table 1, the release of in situ electrons in most events is energy dependent, so a more plausible scenario in these events could be the following: an interchange reconnection happens and leads to upward- and downward-propagating exhausts. Electrons with energy up to 10–20 keV are accelerated near the initial X-point. Further acceleration at both reconnection exhausts leads to electrons of higher energy. For the exhausts propagating downward, the B field and associated turbulence are stronger, so the acceleration time is short leading to no clear energy dependence of HXRs. For the exhausts propagating upward, however, the $B$ field and associated turbulence are weaker, so the acceleration time is longer, leading to a clear energy-dependent release of in situ electrons. In this scenario, the timing of type III radio bursts can be the same as the HXR if the initial X-point

acceleration can accelerate electrons to 10–15 keV, the energy threshold for generating type III radio bursts. If the initial acceleration at the X-point is not powerful enough, then the type III bursts would be later than HXRs. Nevertheless, because the upward-propagating exhausts are associated with further acceleration, we can regard electrons that generate type III radio bursts and those that generate HXRs as different populations. Indeed, an examination of event 9 suggests that this may be the case. In event 9, there are three episodes of type III bursts. The middle episode has a release time of 03:10:53. In comparison, the release time of the 25 keV HXR is 03:09:57; the release time of 26.6 keV in situ electrons is 03:12:25; and the release time of 40.2 keV in situ electrons is 03:15:11. So the type III radio burst release time is ∼1 min later than the 25 keV HXR and is ∼1.5 min earlier than the 25 keV in situ electrons. Since type III radio bursts and 25 keV HXRs are within 1 min, one may regard them to be due to electrons of the same population. However, if the type III radio burst is generated by 15–20 keV electrons, then it is not clear why the type III burst trails the 25 keV HXRs. On the other hand, the type III burst is only 1.5 min earlier than 26.6 keV in situ electrons. Comparing to the fact that 26.6 keV in situ electrons are 2.8 min earlier than the 40.2 keV in situ electrons, it is more likely that the type III generating electrons are of the same population as those in situ electrons, and they lay behind the HXR-generating electrons. Event 18 is similar to event 9. In event 25, the release of in situ electrons also shows clear energy dependence, similar to events 9 and 18, but the 26.6 keV electrons are released ∼6 min later than the type III radio bursts. These three events are further examined in Section 3.2. For the other four events, events 4, 7, 11, and 23, type III bursts had no nearby in situ electrons identified. This is possible if Earth is not magnetically connected to the flare source. Finally, we note that if the initial reconnection is via a closed–closed reconnection and if it triggers an interchange reconnection, as discussed in G. Li et al. (2021) (see also later the Discussion section), then the type III radio bursts will also be trailing the HXRs. In passing, multiple episodes of electron acceleration are likely a common feature of solar flares (Sharma et al., 2020). These authors also suggested that HXR and radio burst sources are likely from electrons in different magnetic loops.

Table 1 contains the main results of our work. In the following, we examine the time delays between the outward- and the downward-propagating electrons in Section 3.1 and discuss the energy dependence of the outward-propagating electrons in Section 3.2. Finally, in Section 3.3, we examine one of the three simultaneous release events in detail.

### 3.1. Time Delay Between Outward- and Downward-Propagating Electrons

We examine the time delay $\Delta t$ between the outward-propagating electrons and the downward-propagating electrons, which is defined as

$$\Delta t = t_{\text{o.e.}} - t_{\text{HXR}} \tag{3}$$

where $t_{\text{o.e.}}$ is the release time of outward-propagating electron from the FVDA (Approach II) and $t_{\text{HXR}}$ is the release time of HXR (as a proxy of release time of downward-propagating electrons). Figures 2 and 3 show the time delay distribution for events in Table 1.

As an estimate of uncertainty, for the downward-propagating electrons, we use both the 12–25 and the 25–50 keV channel of HXR data and Figure 2 (Figure 3) is for the 12–25 keV (25–50 keV) HXR.

Consider first Figure 2. Different panels are for different electron energies. In each panel, the $x$-axis is the time delay $\Delta t$ in seconds and the $y$-axis is the flare class. Different events are marked by the green circles with the event number labeled next to it. Events 14 and 15 are marked by red circles since there is a lack of corresponding flare class information in these two events. In Figure 2, these two events are assigned a B2.0 for clear presentation. Note that the number of events differs in these panels since not all events have in situ electron observations from all six channels. The light blue histogram shown in the inset of each panel is the frequency distribution of the delay time.

From Figure 2, we see that the release time of outward-propagating electrons in all events and all energy channels lag behind the 12–25 keV HXR release time except events 15, 16, and 28 (see below). The delay is mostly distributed within 1,000 s, with a few events having a delay beyond 2,000 s and one event (event 2) having a delay of ∼3,100 s.

For event 15, in situ electron data exist only for four energy channels. Of these, only the 40.2 keV electrons are found to be released earlier than the 12–25 keV HXR. The release time of the 40.2 keV electrons is 03:24:44, with

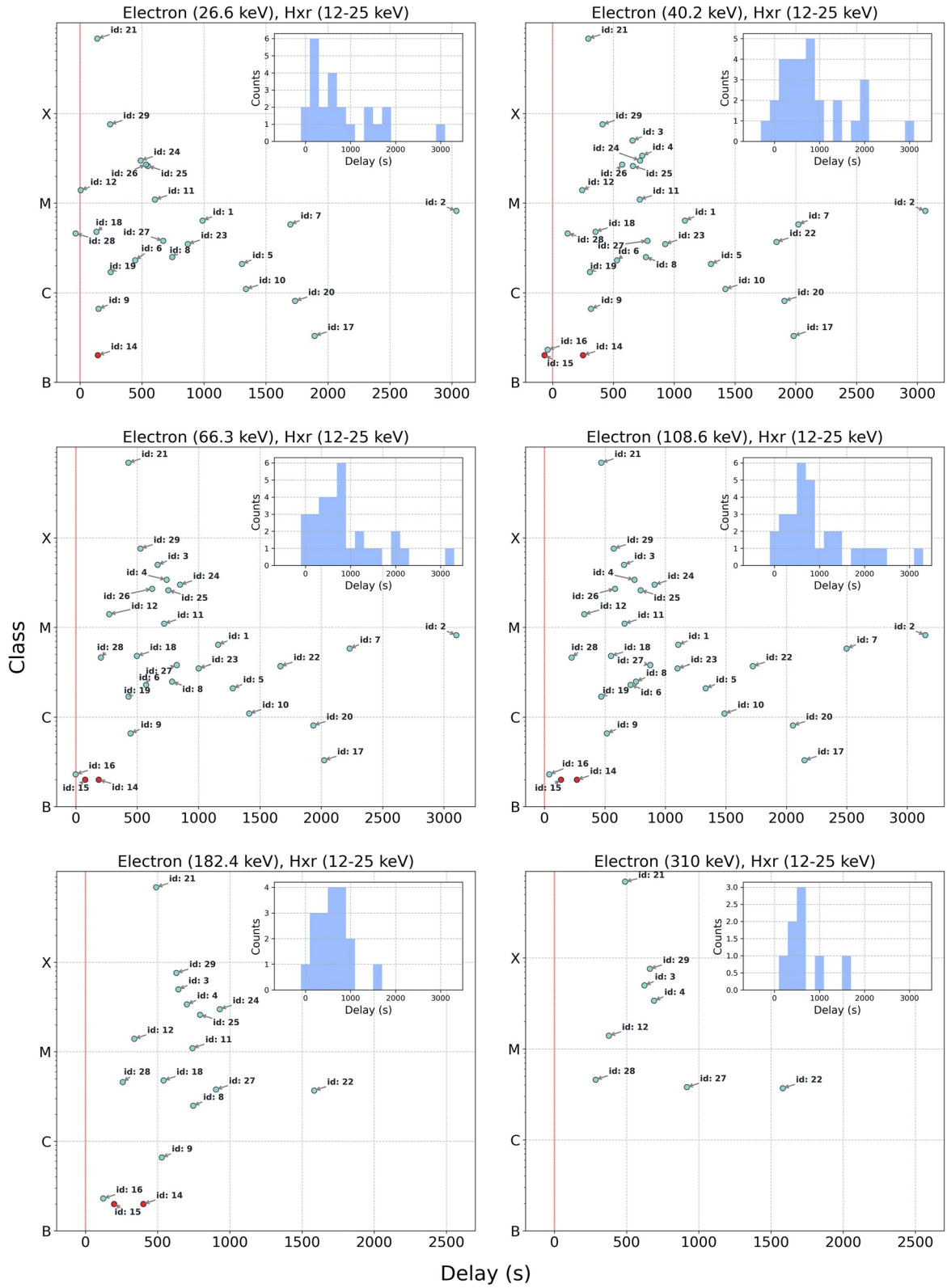


**Figure 2.** Time delay of the release time of in situ electrons from the release time of the 12–25 keV channel of hard X-ray (HXR). Note that both are release times at the Sun. *x*-Axis is the delay time in seconds, and the *y*-axis is the flare class. Event numbers are shown next to the data point. For events 14 and 15, no flare class information was available and an arbitrary B2.0 was assigned. They were labeled by filled red circles.

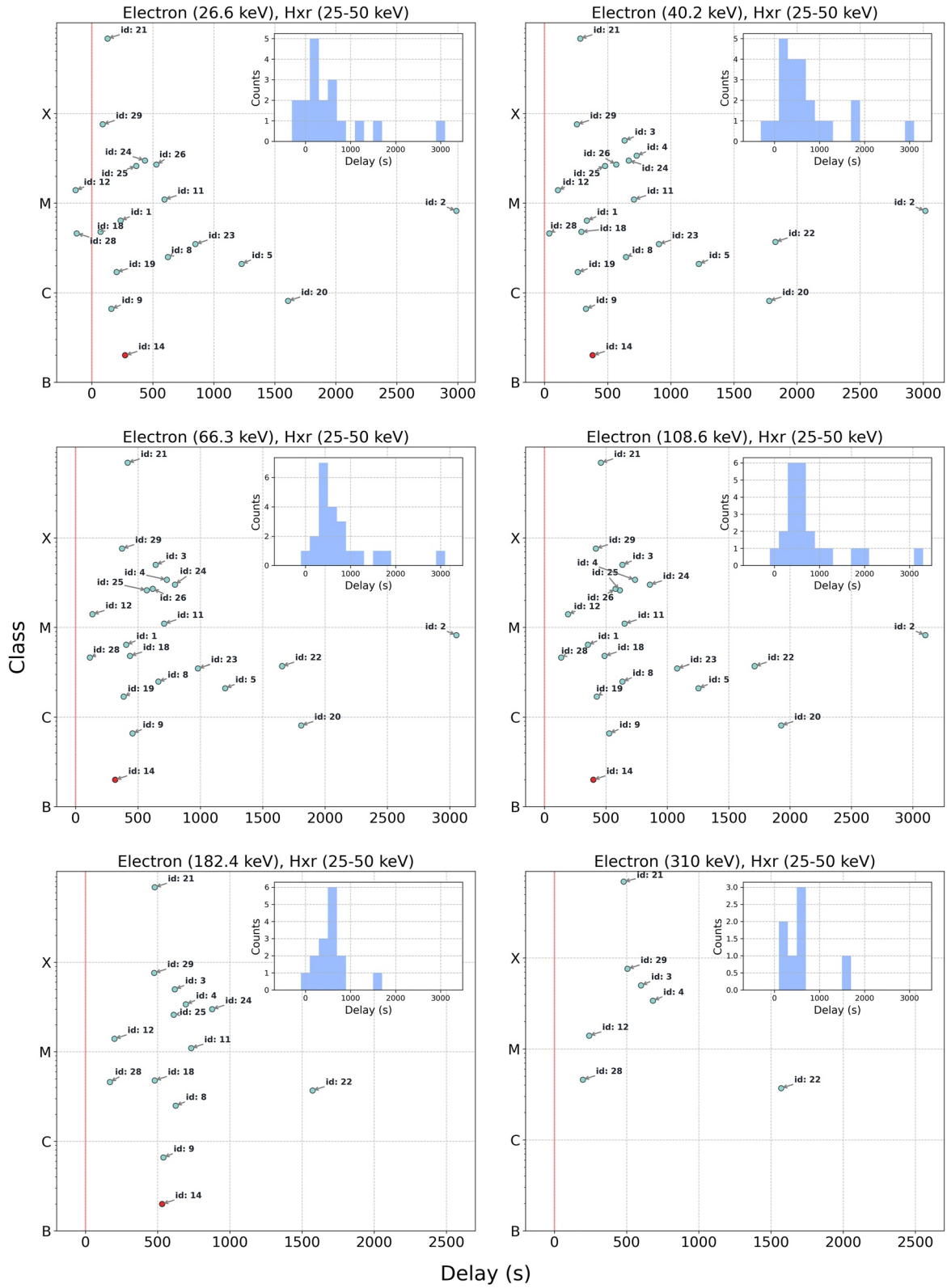


**Figure 3.** Same for Figure 2, but using the 25–50 keV channel instead of the 12–25 keV channel of hard X-ray (HXR) to compute the release time delay.

a ~30 + 42 s uncertainty, where 30 is the intrinsic uncertainty from using the Savitzky-Golay filter and 42 is the uncertainty from the fitting. The release time of 12–25 keV HXR is 03:25:50, with a ~12 s (a smoothing window size of 3 times the time resolution of 4 s) uncertainty. Therefore, the release time delay between the 40.2 keV electrons and the 12–25 keV HXR is consistent with 0. As energy increases, the release times of outward-propagating electrons become clearly delayed from that of the HXR. For event 16, in situ electron data are also only available for four energy channels. The deduced release time of 12–25 keV HXR is 08:20:33, and the earliest $T_r$ of outward electrons is from the 40 keV channel, which is 08:19:48. This yields a delay time of ~−45 s. Considering that the uncertainty of in situ electrons of 40 keV is ~30 + 18 s, and the uncertainty for HXR observation is 12 s, this time delay is also consistent with 0. Furthermore, as energy increases, the release times of outward-propagating electrons become clearly delayed from that of the HXR, as in event 15. For event 28, in situ electron data are available for six energy channels. All in situ electrons except the 26.6 keV channel are released later than the 12–25 keV HXR. The release time for the 26.6 keV outward electron is 21:54:37 with uncertainty ~30 + 13 s and that of the 12–25 keV HXR is 21:55:13 with uncertainty 12 s. Again, taking into account of uncertainty, the time delay is also consistent with 0. For the other five energy channels, the release time of the outward electrons is again significantly later than that of the HXR, similar to events 15 and 16. Therefore, we can conclude that, in these three events, the outward-propagating electrons of lower energy (40 keV in events 15 and 16, 26.6 keV in event 28) are released close in time with the 12–25 keV HXR, and electrons of higher energies (>40 keV) show clear delays from the HXR.

Figure 3 is similar to Figure 2 but using 25–50 keV HXR when calculating the time delay. In only two events, we find that the outward-propagating electrons in the energy channel of 26.6 keV are released earlier (~2 min in both events) than the 25–50 keV HXR. These are events 12 and 28. However, for >50 keV outward-propagating electrons, they are all delayed from the 25–50 keV HXRs. The delays are again mostly within 1,000 s. From Figures 2 and 3, we can conclude that in nearly all events we examine, the outward-propagating electrons are delayed from the downward-propagating electrons of the same energy, and the delay is largely within 1,000 s.

Comparing Figure 2 with Figure 3, we also see that the downward-propagating electrons themselves may be released in an energy-dependent manner. In fact, from Table 1, the downward-propagating electrons of 25–50 keV in event id = 5, 8, 18, 20, 25, 28, and 29 show a clear delayed release relative to those of 12–25 keV, indicating that the acceleration process of the downward electrons may be also time dependent. This is possible, for example, if the downward-propagating electrons are accelerated at a flare termination shock (Guo et al., 2017; G. Li et al., 2013).

To summarize, except for event 13 where an accurate HXR release time cannot be obtained due to a data gap, the outward-propagating electrons of all energy channels in the rest of the 28 events are released consistently later than the downward-propagating HXR-generating electrons. The delay between the outward-propagating electrons and the downward-propagating electrons is largely within 1,000 s. This statistical result can be naturally explained if the acceleration sites of outward- and downward-propagating electrons are different. Different acceleration sites could be the two oppositely propagating reconnection exhausts as proposed in Liu et al. (2013), or for the outward-propagating electrons, a shock wave driven by the jet can be an additional acceleration site besides the reconnection exhaust(G. Li, Zhao, et al., 2020). Note that the fact that the delays are largely within 1,000 s suggests that the acceleration time scale of the outward-propagating electrons is <1,000 s. If a CME-driven shock is involved, assuming a shock speed of ~700–1,400 km/s, the shock moves a distance of 1–2$R_s$ in 1,000 s. So the acceleration of outward-propagating electrons occurs within a few solar radii.

### 3.2. Energy-Dependent Release of Outward-Propagating Electrons

In this section, we examine the energy dependence of the release time of outward-propagating electrons. As explained in the previous section, if the electron release times of any two different energies are within 1 min, the event is classified as an energy-independent release event (which we discuss in the next section), otherwise it is classified as an energy-dependent release event. With this criterion, events 3, 5, and 8 are the only three energy-independent events. The release times for in situ electrons using the FVDA methods for these three events were included in Section 2. Note that relaxing this threshold from 1 to 2 min will increase the number of energy-independent release events to 5. Besides events 3, 5, and 8, events 4 and 26 also become energy-independent release events. More discussions on these events will be given in the next section.

In the work of G. Li et al. (2021), the release times of electrons at different energies (thus different momenta) are compared with that at a reference momentum $p_0$ to yield the release time difference $\Delta t(p, p_0) = t_{\rm rel}(p) - t_{\rm rel}(p_0)$.

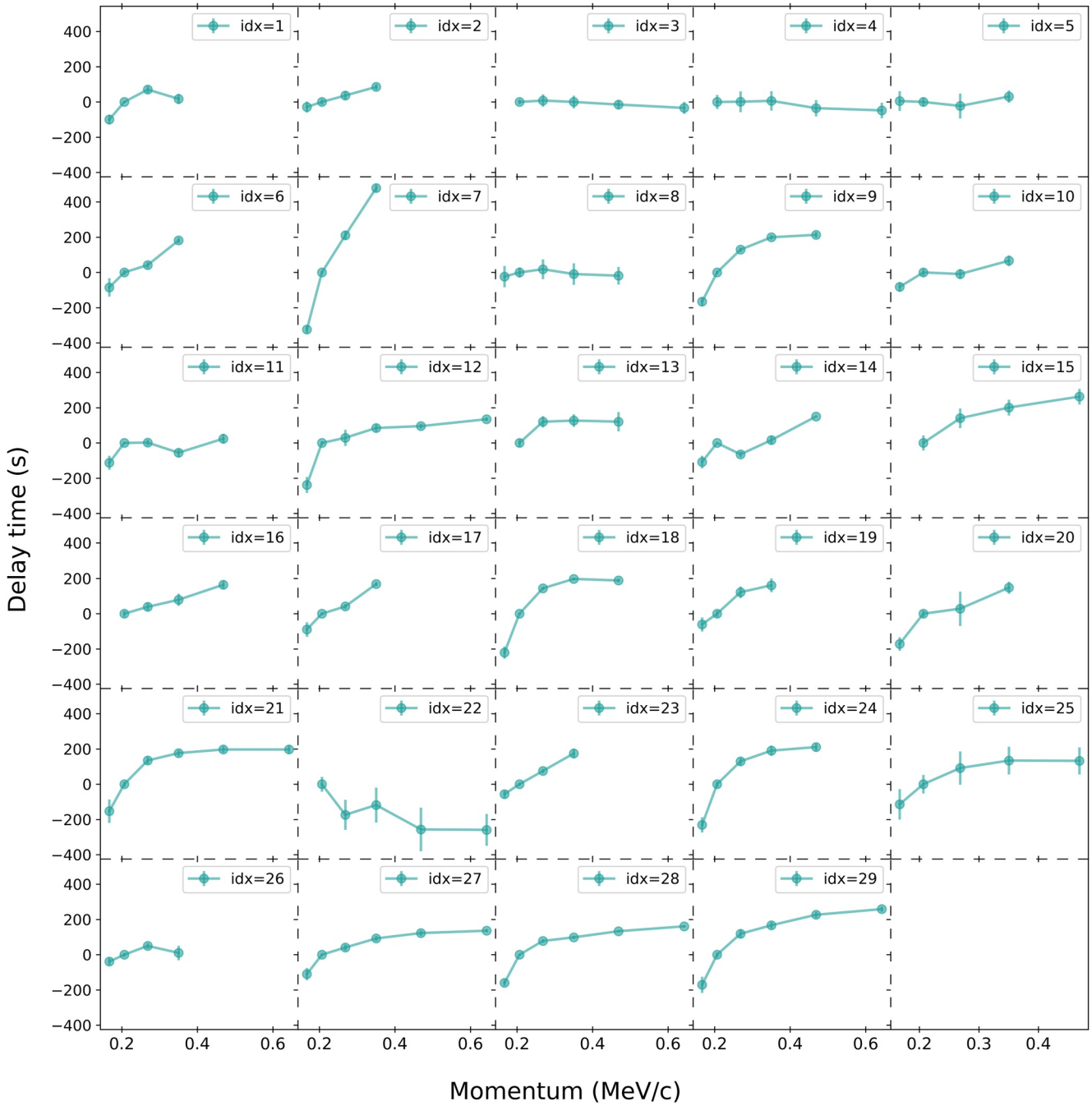


**Figure 4.** The momentum-dependent time delay $\Delta t(p, p_0)$ of outward-propagating electrons with respect to $p_0$. To unify the reference point for all events, $p_0$ is chosen to be 0.207 MeV/c (i.e., $E_0 = 40.2$ keV). Data points are marked as cyan circles. The $x$-axis is electron momentum in unit of MeV/c and the $y$-axis is the time delay in seconds. The uncertainty of the $\Delta t(p, p_0)$ is the sum of the uncertainty in the release time of the electron with momentum $p$ and the electron with momentum $p_0$.

We follow G. Li et al. (2021) in obtaining the release time difference $\Delta t(p, p_0)$. Figure 4 shows the momentum dependence of the time difference $\Delta t(p, p_0)$ for all 29 events. The reference momentum $p_0$ is 0.207 MeV/c for all events. In Figure 4, the error bar of each point represents the uncertainty derived from electron release times. Assuming the release time of electrons is $t_r(p) = t(p) \pm u(p)$, the time difference can be expressed as $\Delta t(p, p_0) = (t(p) - t(p_0)) \pm (u(p) + u(p_0))$, where $p_0$ corresponds to the reference momentum and $(u(p) + u(p_0))$ represents the deduced uncertainty of $\Delta t(p, p_0)$. We can see that the uncertainty of the time delay for most points is smaller than the data symbol. For the majority of these points, the uncertainty is smaller than 60 s.

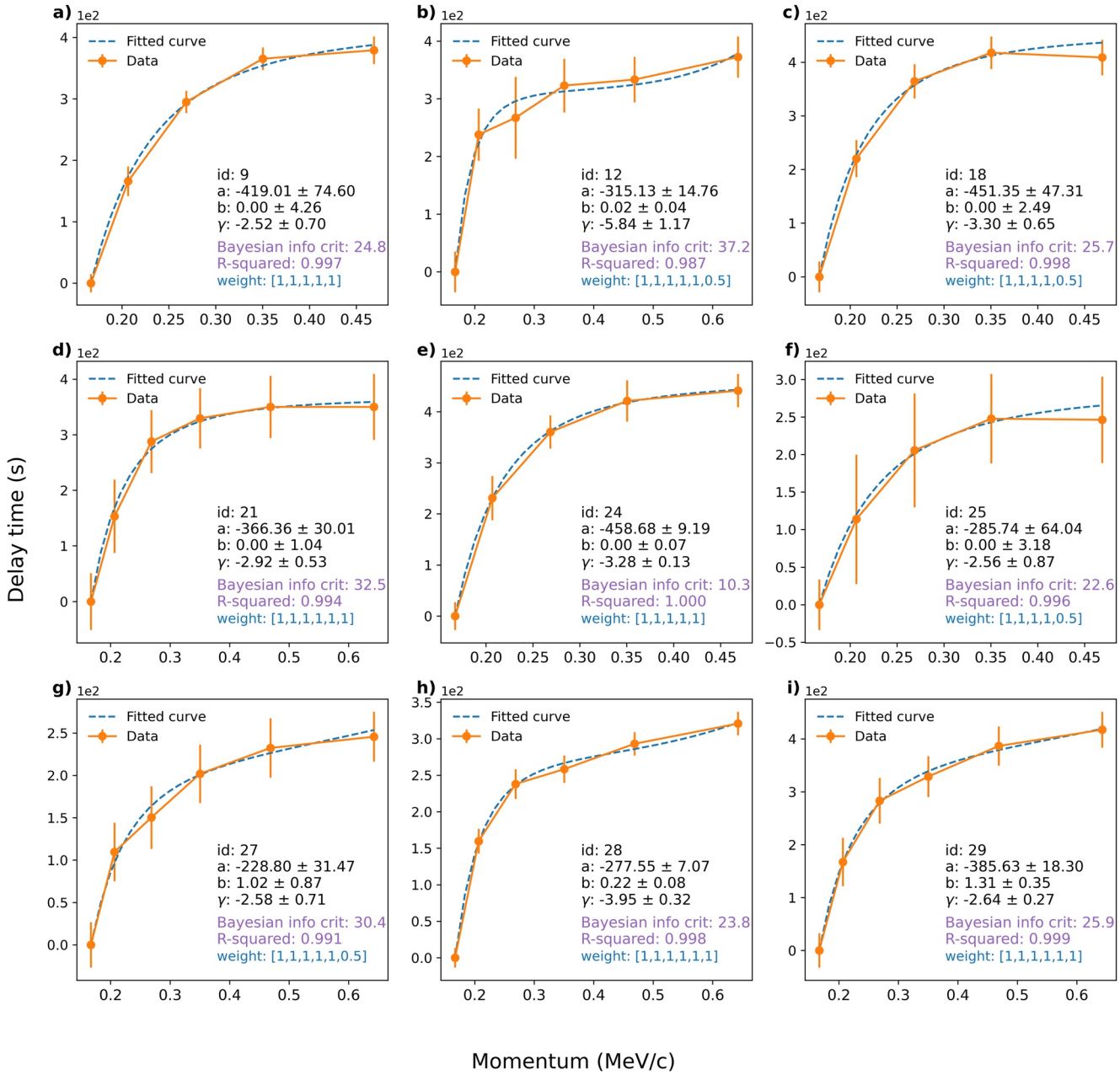


**Figure 5.** The momentum dependence of the release time difference $\Delta t(p, p_0)$ with $p_0 = 0.167$ MeV/c. Only events with five or more data points are fitted. The orange filled circle is the data and the blue dashed line is the fitting. The $x$-axis is electron momentum in unit of MeV/c and the $y$-axis is the time difference in seconds (note that the $y$-axis values are to be multiplied by a factor of 100, as indicated in the upper left corner of the panels). The uncertainty of the $\Delta t(p, p_0)$ is the sum of the uncertainty in the release time of the electron with momentum $p$ and the electron with momentum $p_0$.

As can be seen from Figure 4, $\Delta t(p, p_0)$ for many events show similar momentum dependence. Assuming this time difference is caused by acceleration and trapping, G. Li et al. (2021) has proposed to fit the release time difference as a function of electron momentum by

$$\Delta t(p, p_0) = \text{sign}(\gamma) a \left[ \left( \frac{p}{p_0} \right)^{\gamma} - 1 \right] + b \left[ \left( \frac{p}{p_0} \right)^{-\gamma} - 1 \right] \quad (4)$$

Here, $p$ is the momentum of electrons; $p_0$ is the reference momentum and is chosen to be the lowest energy channel for a given event. According to our event list, the lowest energy of electrons for an event is either 26.6 keV

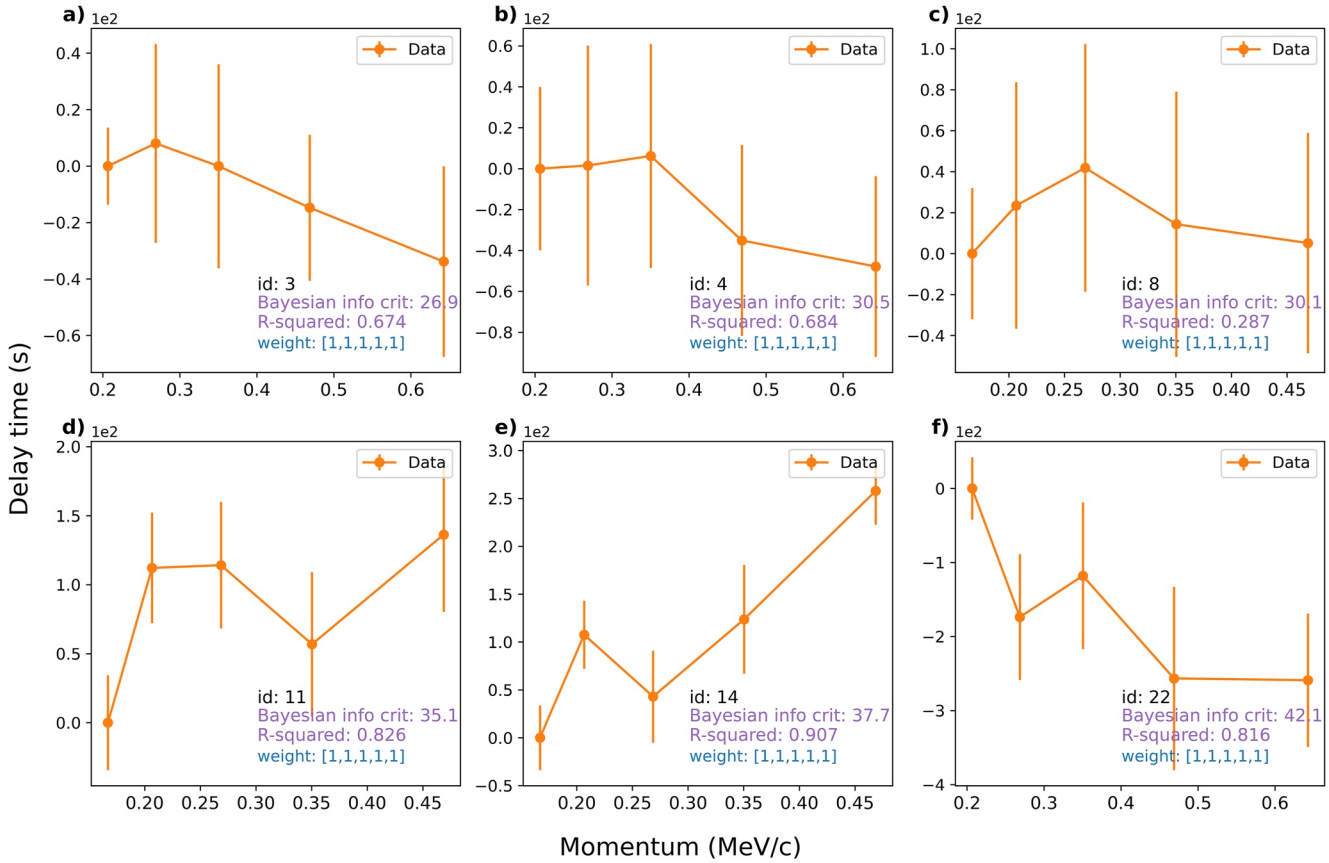


**Figure 6.** Similar to Figure 5, but for events that cannot be fitted by Equation 4.

(corresponding to $p_0 = 0.167$ MeV/c) or 40.2 keV (corresponding to $p_0 = 0.207$ MeV/c). In the right side of Equation 4, the first term is due to acceleration, and the second term is due to escape/trapping, both of which are functions of the spatial diffusion coefficient $\kappa(p)$, which we assume to have momentum dependence as $\sim p^{\gamma}$ (G. Li et al., 2021). If we further assume the spectrum of the broad-band turbulence can be approximated as $\kappa^{-\epsilon}$, then under the framework of quasi-linear theory (Jokipii, 1966), the spectral index $\epsilon$ satisfies $\gamma = 3 - \epsilon$. Hence, we can probe the nature of the turbulence at the flare site using the fitting parameter $\gamma$.

**Table 2**
*The Fitted $\gamma$ Value as in Equation 5*

| Id | Date | $\gamma$[a] | Class | $R^2$ | BIC |
|---|---|---|---|---|---|
| 9 | 2004-02-28 | $-2.52 \pm 0.70$ | B6.6 | 0.997 | 24.8 |
| 12[b] | 2005-05-16 | $-5.84 \pm 1.17$ | M1.4 | 0.987 | 37.2 |
| 18 | 2011-05-15 | $-3.30 \pm 0.65$ | C4.8 | 0.998 | 25.7 |
| 21[b] | 2011-08-09 | $-2.92 \pm 0.53$ | X6.9 | 0.994 | 32.5 |
| 24 | 2014-02-20 | $-3.28 \pm 0.13$ | M3.0 | 1.000 | 10.3 |
| 25 | 2014-03-28 | $-2.56 \pm 0.87$ | M2.6 | 0.996 | 22.6 |
| 27[b] | 2014-06-12 | $-2.58 \pm 0.71$ | C3.8 | 0.991 | 30.4 |
| 28[b] | 2016-07-20 | $-3.95 \pm 0.32$ | C4.6 | 0.998 | 23.8 |
| 29[b] | 2016-07-23 | $-2.64 \pm 0.27$ | M7.6 | 0.999 | 25.9 |

[a]$P_0 = 0.167$ MeV/c, $\eta = 0$. [b]Events with six data points.

Equation 4 contains four parameters: $p_0$, $a$, $b$, and $\gamma$; therefore, to have a meaningful fitting, we only consider events with five or more data points, leading to a total of 15 events (see Figure 4). Of these, nine events can be fit reasonably well by Equation 4 and these are shown in Figure 5. The remaining six events do not yield reasonable fitting and are shown in Figure 6.

In Figure 5, the data are shown as the orange dot and the fitted curve is shown as the blue dashed line. The coefficient of determination ($R^2$) and the Bayesian information criterion (BIC) are also obtained. Both $R^2$ and BIC are indicators of the goodness of the fitting. The range of $R^2$ is from 0 to 1 and $R^2 = 1$ represents a perfect fitting. We require $R^2$ to be larger than 0.98 to consider it an acceptable fitting. The BIC is a useful statistical measure for model selection, taking overfitting into account. When multiple models (often of similar kind but with different parameters) are adopted for a fitting, the one with lower BIC is generally preferred. In our fitting, we examine how the BIC varies by allowing the data points for different energy bins to have different weights. This is to capture the fact that the quality of electron profiles for different energy bins is different. Generally, the electron time intensity

profiles of higher energy, for example, 182.4 or 310 keV, have larger fluctuations than those at lower energies so that they may correspond to a lower weight. For simplicity, the weight of each data point is set to be either 1 or 0.5. If one tenth of the peak flux (corresponding to $\eta = 0.1$) is lower than the average pre-event background $+3\sigma$, a weight of 0.5 will be assigned to that energy channel. Otherwise, the weight is set to be 1. Whether or not the weight of a specific delay time is set to 0.5, it has little impact on the value of $\gamma$. Taking panel (g) as an example, if we do not decrease the weight of the last data point, the value of $\gamma$ becomes $-2.5 \pm 0.68$ from $-2.58 \pm 0.71$, the $R^2$ remains 0.991, and BIC changes to 30.6 from 30.4. This shows that the choice of a nonuniform weight does not affect our fitting result, indicating the robustness of the fitting results.

In all panels of Figure 5, the parameter $b$ is consistent with 0, that is, the delay due to trapping is negligible. This means that Equation 4 can be simplified to be

$$\Delta t(p, p_0) = \mathrm{sign}(\gamma) a \left[ \left( \frac{p}{p_0} \right)^{\gamma} - 1 \right] \tag{5}$$

Clearly parameter $a$ is an overall amplitude, and the shape of the curve is completed decided by the parameter $\gamma$. The fitting result of $\gamma$ for these nine events are summarized in Table 2. Events with six data points are marked by the "b" symbol.

Figure 6 is similar to Figure 5, but for events that cannot be fitted by Equation 4. For these events, we find that although the uncertainty of the time delay $\Delta t(p, p_0)$ is smaller than 60 s, it is still relatively large compared to the value of $\Delta t(p, p_0)$. In events 3, 4, and 8, the uncertainty of the $\Delta t(p, p_0)$ exceeds the value of $\Delta t(p, p_0)$, which implies that a clear energy dependence of the release time for these events cannot be obtained. Taking event 8 (corresponding to panel c) in Figure 6 as an example, electrons of 0.167 MeV/c (i.e., $E_0 = 26.6$ keV) are released at 13:12:22 $\pm$ 32.0s, and electrons of 0.269 MeV/c (i.e., $E_0 = 66.3$ keV) are released at 13:13:01 $\pm$ 28.4s. The deduced time delay $\Delta t$(0.269 MeV/c, $p_0$) with respect to $p_0 = 0.167$ MeV/c is therefore 39 $\pm$ 60.4 s. This means that within the uncertainty, electrons of these two energies are released simultaneously. In Figure 6c, all the data points have $\Delta t(p, p_0)$'s uncertainty greater than its value, therefore the electrons of different energies can be regarded as released at the same time. This explains why the release times cannot be well fitted by Equation 4 or 5 for this event. Events in panels (a) and (b) have the same pattern with event 8 in panel (c). In Figures 6d and 6e, $\Delta t(p, p_0)$'s uncertainty becomes smaller than its value. Although electrons of higher energies are generally released later, the time delay is not a convex function, but bends at a certain momentum above $p_0$. This is possible if the diffusion coefficient does not have a momentum dependence given by $p^{\gamma}$ or if the acceleration process is not governed by a diffusion process (e.g., it may be governed by a DC electric field acceleration).

Figure 6f is event 22. Of all 29 events, event 22 is the only event in which high-energy electrons are released earlier than low-energy electrons when a nominal Parker field length is used. If one assumes, as in other events, that high-energy electrons are released at the same time or later than low-energy electrons, then a path length longer than the nominal Parker field path length has to be assumed. In fact, the path length from Approach I for this event is 1.51 au. Using this path length, the release times between different energy channels are within 123 s. We note that the rising phases of electron time intensity profiles in this event are more gradual than in other events. This can be caused by distorted IMF due to large scale structures in the solar wind, for example, a preceding CME, which can lead to a longer path length. Therefore, it is possible that in this event, electrons are released similarly in time and they propagate along a magnetic field that is non-Parker and having a path length $\sim$1.5 au. Such a scenario is not unheard of and has been discussed in G. Li, Wu, et al. (2020).

The distribution of $\gamma$ and its dependence on the solar flare class and the relative release time delay is shown in Figure 7. The light blue histogram in the right panel is the distribution of $\gamma$. The $\gamma$ is mainly distributed between $-3.5$ and $-2.5$ and shows no clear correlation with the flare class and the delay time. Event 12 has a $\gamma = -5.84$ which is significantly smaller than the gamma value of other eight events. From Figure 5 we see that event 12 has a $R^2 = 0.987$, the smallest of all nine events in Figure 5. Since $\epsilon = 3 - \gamma$, we can infer that $\epsilon$ is mainly distributed between 5.5 and 6.5. As pointed out in G. Li et al. (2021), an $\epsilon$ steeper than 3 (corresponding to the nominal value for the dissipation range turbulence), is consistent with a scenario of magnetic reconnection in the reconnection exhaust. In the work of Vech et al. (2018), the authors found that the turbulence spectrum can be significantly steepened from 3 at the beginning of the dissipation range due to the generation of vortex-like structures, which are triggered by magnetic reconnection. This phenomenon of structure disruption significantly accelerates the turbulence cascading process and to maintain a constant energy cascading rate a steeper spectrum must develop. These

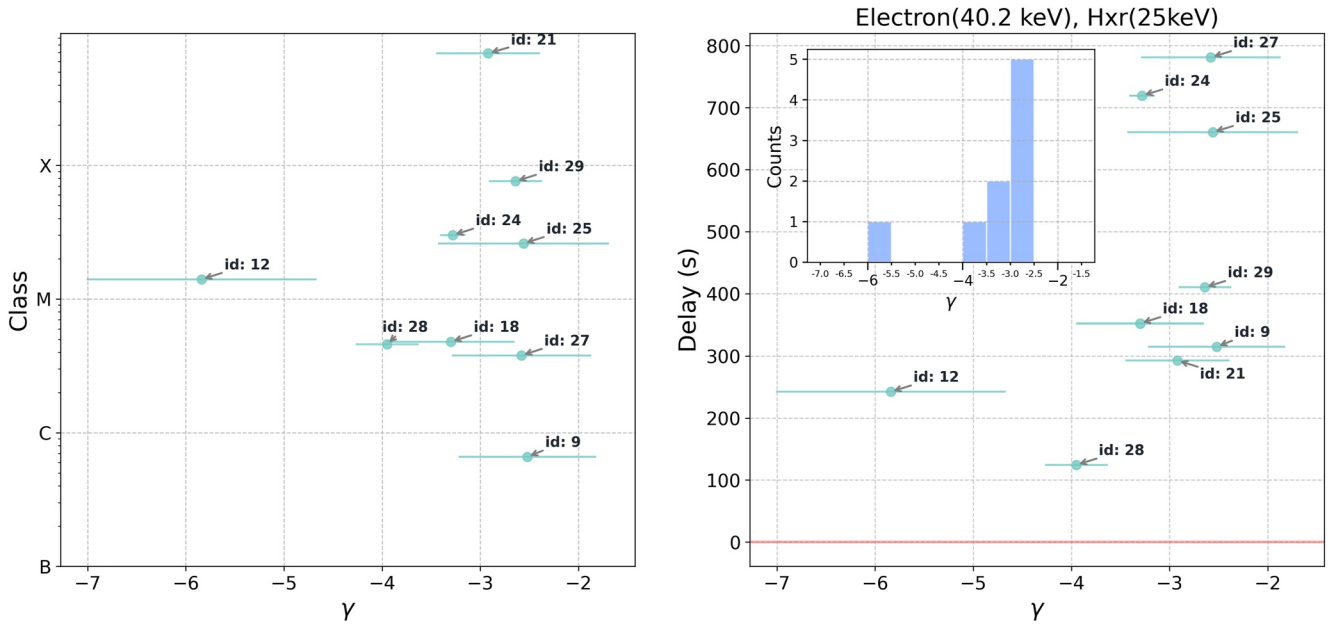


**Figure 7.** The distribution of the $\gamma$ value for the nine events shown in Table 2. The $y$-axis in the left panel is the flare class and the $y$-axis in the right panel is the relative release time delay $\Delta t(p, p_0)$.

vortex-like structures can lead to large nonthermal velocity at the reconnection site. Using the Fe XXIV 192.03 Å line broadening, Y. Li et al. (2018) inferred a large nonthermal velocity in the SOL2017-09-10T16:06 flare, consistent with Vech et al. (2018). Our result of a $\epsilon$ ranging between 5.5 and 6.5 also supports Vech et al. (2018). Note that event 29 was the event examined by G. Li et al. (2021). In G. Li et al. (2021), a $\gamma = 5.1$ was obtained. This is to be compared with this work where we find $\gamma = 5.64 \pm 0.27$. The difference is mainly due to the selection of the background. In G. Li et al. (2021) the background period was chosen to be the same for different energy channels for a fixed 10 min which was 05:18–05:28(HH:MM). This period however, overlaps with the rising phases for the 182 and 310 keV electrons. Consequently this leads to a smaller $\gamma$ in (G. Li et al., 2021). In the current work, we use different background periods for different energy channels.

### 3.3. Energy-Independent Release of Outward-Propagating Electrons

If the electron release times of different energies in one event are within 1 min, the event is classified as an energy-independent release event. Three events out of 29 events are energy-independent release events. These are events 3, 5, and 8 in Table 1. The release times of HXRs and in situ electrons for these three events are shown in Figure 1. Because these events differ from the rest of the events, in the following, we take a closer look of both the remote sensing and in situ observations of event 3 as an example.

Figure 8 shows the magnetogram of the AR 10069 in the left panel, and the HXR intensity from 01:05 to 02:00 UT for three energy channels in the right panel. The AR is located at a longitude of western 40°, therefore is magnetically well connected to the Earth along the nominal Parker field (see below). In the right panel, the segments in red indicate the backgrounds from 01:10:00 to 01:25:00 UT. The onset and peak times of the HXR are labeled as the orange "diamond" and green "triangle," respectively. The onset times for HXR-generating electrons of 12–25 and 25–50 keV are determined to be 01:33:42 and 01:34:06 UT.

In Figure 9, the left panel shows the electron time intensity profile for five energies. The reference points marked as "triangle," "square," "circle," and "diamond" correspond to $\eta = 0.5$, 0.35, 0.2, and 0.06, respectively. The right panel shows the FVDA analysis for the four $\eta$s. The nominal Parker field length of this event is 1.11 au with a solar wind speed $V_{sw} = 508.4$ km/s, the average of an 8-hr period that is 2 hr prior to the arrival of the in situ electrons. Using Equation 1, the onset times $t_0(\eta = 0)$ are 02:00:51 ± 13, 01:56:13 ± 21, 01:52:35 ± 22, 01:49:41 ± 12, and 01:47:30 ± 20 s for electron energies of 40, 66, 109, 182, and 310 keV, respectively. Therefore, the path length $L$ calculated from $t_0(\eta = 0)$ is 1.15 ± 0.02 au, which is very close to the Parker value, suggesting that the field line

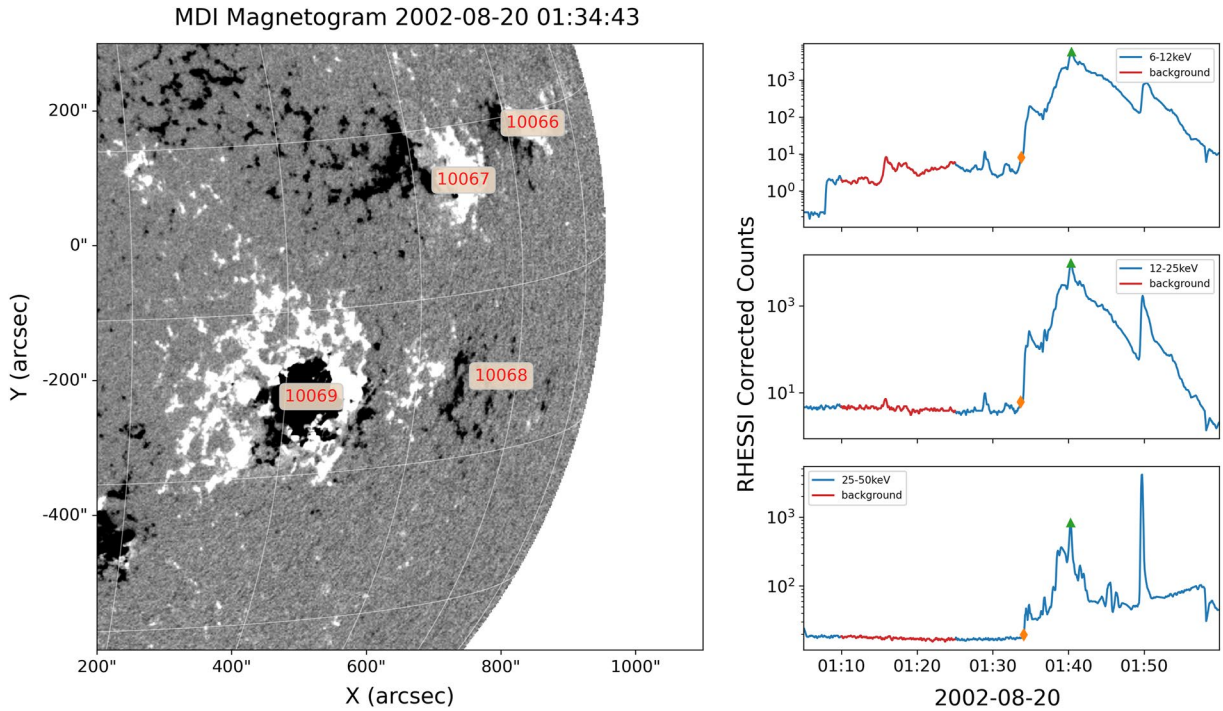


**Figure 8.** (left) Magnetogram of the 2002-08-20 event. The source region of the flare is AR10069. (right) The Ramaty High Energy Solar Spectroscopic Imager (RHESSI) hard X-ray ( HXR) time profile. The background period is shown by the red segment.

in this event does not deviate much from the nominal Parker field. As shown in Figure 1, choosing a path length of 1.15 and 1.06 au and using Equation 2, we still find that the $T_r$ for electrons of different energies are consistent with a simultaneous release.

An energy-independent release of outward-propagating electrons could be due to a very fast electron acceleration directly at the magnetic reconnection site (see e.g., PIC simulations by X. Li et al. [2017]). It is tempting to invoke the interchange reconnection scenario as proposed in Heyvaerts et al. (1977) and Krucker et al. (2007) for this event. However, as shown in Figures 2 and 3, there is a time delay (>500 s) between the outward- and the downward-propagating near-relativistic electrons, which is hard to explain if the interchange reconnection is responsible for both the downward- and outward-propagating electrons. One possible explanation of the delay is that a solar flare is intermittent and can have multiple episodes of magnetic reconnection and which can occur at different locations. The outward-propagating electrons may correspond to one of many episodes but not the very first episode of the magnetic reconnection process. If the very first episode of the magnetic reconnection is of closed–closed reconnection instead of interchange reconnection, then there will be only HXRs associated with the first episode of the reconnection but not in situ electrons. If a subsequent interchange reconnection occurs and the open field line is magnetically connected to the Earth, then electrons accelerated at the earlier closed–closed reconnection site can access these open field lines and be observed in situ at 1 au. Indeed, recent observations of HXR and microwave suggested that multiple episodes in a solar flare are not uncommon (Battaglia et al., 2021; Sharma et al., 2020).

Event 3 has been examined previously by Krucker et al. (2007). In that study, the authors used the traditional VDA to obtain estimates of the release time of in situ electrons at the Sun and an event is defined to be a prompt event if this release time coincides with the HXR burst time. Krucker et al. (2007) classified this event as a prompt event. However, the VDA method contains large uncertainty in obtaining the release time of in situ near-relativistic electrons at the Sun. In this work, by using FVDA, we find a clear delay of >500 s between the release time of in situ electrons and the release time of 12–25 and 25–50 keV HXRs. Our work shows that for comparative studies between in situ electrons and HXRs, it is important to use the FVDA to obtain accurate estimates of electron release times at the Sun.

We use 1-min as the threshold for determining if the release of in situ electrons is energy dependent or energy independent. One relevant question one can ask is how much does the result depend on this choice of threshold?

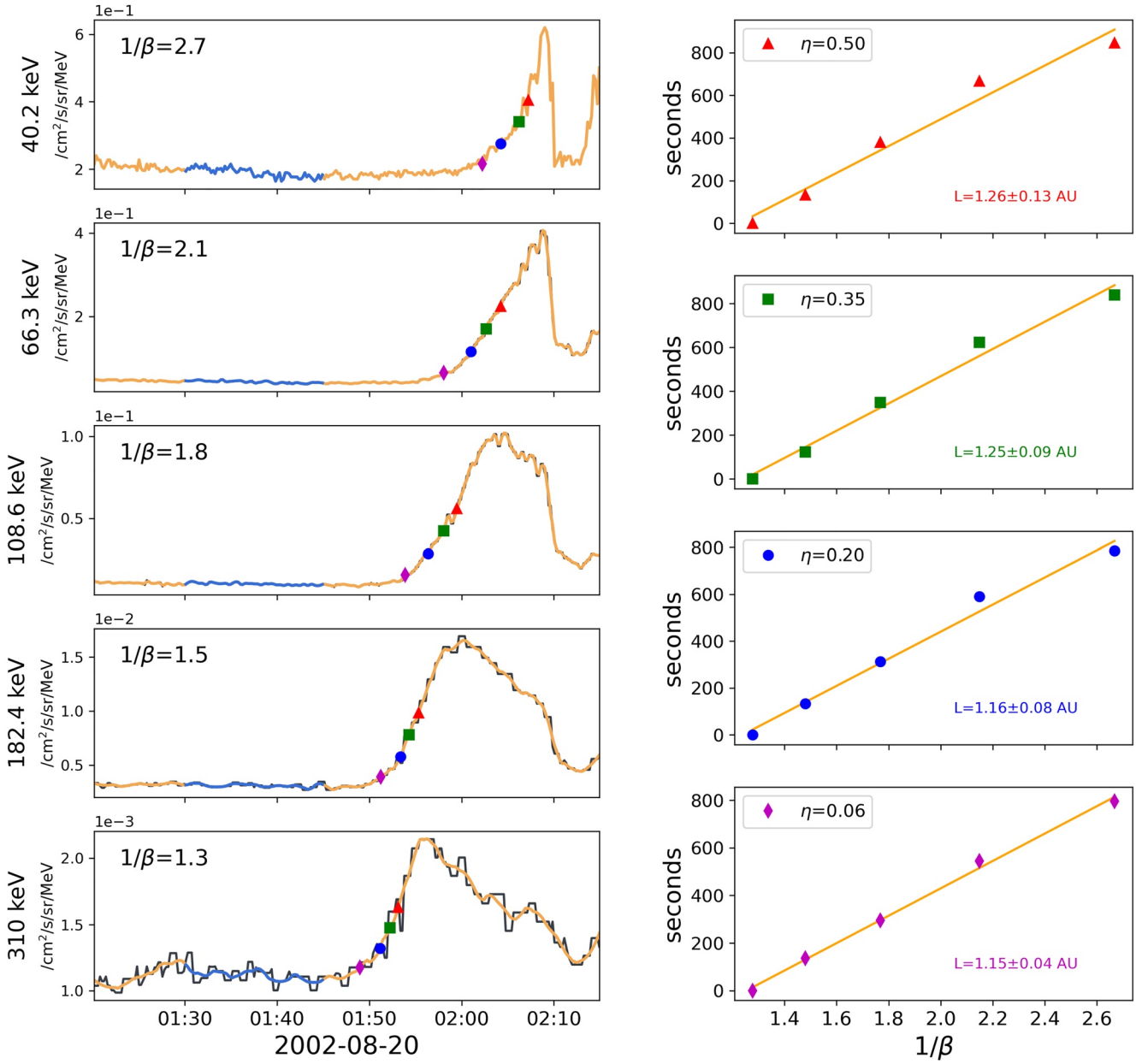


**Figure 9.** (left) In situ electron time intensity of the 2002-08-20 event. Data for five energy channels are available for this event. Data from WIND/3DP are shown as the black curve and the yellow curve is after applying the Savitzky-Golay filter. For the two lowest energy channels, the black curve is overlapped by the yellow curve. (right) The fraction velocity dispersion analysis (FVDA) results for four different $\eta$. As $\eta$ decreases, the path length also decreases and approaches the nominal Parker field path length.

If we relax this threshold to 2 min, as shown in Figure 4, we find that events 2, 4, and 26 will also become energy-independent release events. However, event 2 only has data from four energy channels, and the release times for these four energy channels show a monotonous increase with electron energy. If this energy dependence continues to a higher energy channel, then the release time difference between this energy channel and the lowest energy channel can exceed 2 min. So event 2 may or may not be classified as an energy-independent release event. For event 4, the path length from Approach I is 1.32 ± 0.04 au. This is to be compared with the Parker field path length of 1.11 au in Approach II. The difference, 0.21 au, is larger than those in events 3, 5, and 8. Nevertheless, when relaxing the threshold to 2 min, the release time differences for both a path length of 1.11 and 1.32 au are within 2 min, making event 4 an energy-independent release event. For event 26, the path length from Approach I is 0.99 ± 0.02 au, consistent with 1.0 au, and the Parker path length is 1.10 au. Relaxing the threshold to 2.0 min,

release time differences from both Approaches I and II in event 26 are also within the threshold (2 min). So event 26 also becomes an energy-independent release event. In summary, when increasing the threshold to 2 min, a total of five events can be classified as energy-independent release events. We remark that the choice of the threshold should be larger than but close to the uncertainty of the release times. The FVDA method provides a measure of the uncertainty of the release time. As we discussed earlier, this uncertainty contains an intrinsic 30-s uncertainty from the time resolution of in situ electron data and applying the Savitzky-Golay filter; as well as a fitting uncertainty that is often ∼20 s. Therefore our choice of a 1-min threshold is appropriate.

## 4. Conclusions

In this article, we perform a statistical study of the release time for 29 impulsive SEE events from 2002 to 2016 using in situ electron data from WIND/3DP and HXR observation from RHESSI and Fermi/GBM. Based on the recently developed FVDA (Zhao et al., 2019), we examined the release time of both the outward- and downward-propagating near-relativistic electrons and showed that for all events, there is a distinct time delay, mainly distributed between 0 and 1,000 s, which is consistent with the case study of G. Li, Zhao, et al. (2020) and G. Li et al. (2021). The release time of in situ electrons also shows clear energy dependence with higher energy electrons released later, consistent with a time-dependent acceleration process. For 28 events where type III radio bursts are available, we also compare the release time of type III radio bursts and the release times of in situ electrons. In 15 events, the timing of type III radio bursts is consistent with that of low-energy electrons. In 11 (2) events, the timing of type III radio bursts is earlier (later) than the release of in situ electrons. In 7 out of these 11 events, the timing of type III radio bursts is consistent with the HXR. Our results suggest that a delayed release of in situ electrons compared to HXR is a common phenomenon and the HXR-generating electrons and the in situ electrons are likely of two different populations in a majority of the events we examined. This finding is consistent with the scenario where electrons can be accelerated at both the outward- and downward-propagating exhaust as proposed by Liu et al. (2013). Using a threshold of 1 min, 26 of the 29 events (i.e., ∼90%) show clear energy-dependent release for outward-propagating electrons; in only one of these events (event 22), we find that high-energy electrons are released earlier than low-energy electrons and in the other 25 events high-energy electrons are released later than low-energy electrons; in events 3, 5, and 8, that is, 3 of the 29 events (∼10%), electrons of different energies are released within 1 min, showing no energy dependence. If we relax the duration threshold from 1 to 2 min, then events 4 and 26 now become energy-independent release events, making the total number of energy-independent release events to 5. In the 26 events that show energy-dependent release, 15 have electrons from five or more energy channels. For these events, we extend the analysis of G. Li et al. (2021) and fit the release time as a function of electron momentum by a power law as given by Equation 5. The fitting parameter $\gamma$ mainly distributed between $-3.5$ and $-2$, which corresponds to a turbulence spectrum $\sim k^{-6.5}$ to $k^{-5}$ at the acceleration site. Such a spectrum may indicate a dissipation range. The value of $\gamma$ shows no correlation with the flare class and the delay in electron release time.

One important result from this study is the identification of three events (3, 5, and 8) in which in situ electrons are released simultaneously at the Sun but later than HXR-generating electrons. These are events that satisfy the implicit assumption of the VDA. However, the occurrence rate of these events is low, only ∼10%. The reason for this low frequency remains to be investigated.

One of the assumptions of the FVDA is the scatter-free assumption. This is a reasonable assumption if the electron path length is shorter than the electron mean free path. However, for events where electron's mean free path is comparable to the path length, the effect of scattering is important and has to be considered. In a recent work, Dröge et al. (2018) examined the 20 October 2002 event using a numerical approach which took pitch angle scattering of electrons into account. The pitch angle scattering diffusion coefficient $D_{\mu\mu}$ has both radial and energy dependence. By working with level zero data from WIND/3DP and by comparing simulation with the observation, they suggested that a scatter-free assumption tends to work better for low-energy electrons than high-energy electrons. In another study, Tan et al. (2011) discussed the cause of the scatter-free transport of nonrelativistic solar electrons. They examined the energy dependence of electron angular distributions and related it with the steepening of IMF power spectral densities, concluding that the scattering of energetic electrons (and protons) is energy dependent. These studies signify the importance of the role of numerical simulation in understanding in situ electron observations. It also implies that if we can observe impulsive events from a much closer distance than 1 au, then the propagation effect can be minimized. Recently, two heliospheric missions,

namely Parker Solar Probe (PSP) and Solar Orbiter (SolO) have made considerable progress in observing SEP events. Observing the Sun from as close as $10R_s$ (PSP) and off the ecliptic plane (SolO), they are expected to see many more events with higher fluence and more details. Applying the FVDA method to these events will therefore have lower timing uncertainties than to events at 1 au. This will help us to learn more about the underlying particle acceleration and release process. Together with observations at 1 au, we may even have the opportunity to observe the same event from multiple spacecraft. Such a rare opportunity will help us to better understand the role of transport (pitch angle scattering) and to better decipher the energy dependence of the release time delay. As mentioned in Section 3.3, we suggest a possible scenario in which the flare-driven reconnection between closed loops serves as a trigger of interchange reconnection, and an energy-independent release event can only be observed if the interchange reconnection is successfully induced and the open field line is well connected to the Earth. In these events, the observed delay between in situ electrons and the downward-propagating electrons is possible if the in situ electrons do not correspond to the first episode of HXR. Since the time profiles of HXR represent spatially integrated solar atmosphere response to the precipitating electrons, the first episode of HXR represents the earliest precipitating electrons. Since the interchange reconnection does not occur at the very beginning of a flare, the release time of in situ electrons is thus delayed from the onset time of the first HXR episode.

In a recent paper, W. Wang et al. (2021) examined the spectral relationship between HXR-producing electrons and SEEs and also concluded that the HXR-producing electrons and SEE electrons are of two different populations. They also suggested that two (or more) reconnection processes may occur at the reconnection site, and the HXR-generating electrons are electrons that experience two consecutive accelerations, that is, they are downward-traveling electrons produced at the first reconnection site which occur high in the corona. Such a two-stage acceleration is consistent with our current study. Note that W. Wang et al. (2021) suggested that the HXR-generating electrons may occur after low-energy (<30 keV) outward SEEs. However, if the acceleration at the first reconnection site is not powerful, then outward-propagating SEEs would also need to experience a secondary acceleration, therefore lag behind the HXRs, as found in this paper. To further understand the electron acceleration process at a flare, the energy-independent release events, although rare, may yield valuable clues. Detailed studies of these events will be reported in the future.

## Data Availability Statement

All data used in this work are publicly available at the CDAWeb database (https://cdaweb.gsfc.nasa.gov/index.html/). All event analysis data presented in the paper are archived in a data set on Zenodo. The doi is https://doi.org/10.5281/zenodo.7410328.

**Acknowledgments**
XYW and SY are supported by a NSFC grant under contract no. 42074204. GL acknowledges an UAH PI support. LW is supported in part by NSFC under contracts 42127803 and 42150105, in part by the China National Space Administration project (D020301). FE appreciates DFG support SFB1491. GL, SY, LW, and FE also acknowledge supports from the ISSI Team 469. Constructive suggestions from both referees are greatly appreciated.

## References

Anderson, K. A., Sommers, J., Lin, R. P., Pick, M., Chaizy, P., Murphy, N., et al. (1995). Mirroring of fast solar flare electrons on a downstream corotating interaction region. *Journal of Geophysical Research*, *100*(A1), 3–11. https://doi.org/10.1029/94JA01811

Baba, K., Bahi, L., & Ouadif, L. (2014). Enhancing geophysical signals through the use of Savitzky-Golay filtering method. *Geofísica Internacional*, *53*(4), 399–409. https://doi.org/10.1016/S0016-7169(14)70074-1

Battaglia, M., Sharma, R., Luo, Y., Chen, B., Yu, S., & Krucker, S. (2021). Multiple electron acceleration instances during a series of solar microflares observed simultaneously at X-rays and microwaves. *The Astrophysical Journal*, *922*(2), 134. https://doi.org/10.3847/1538-4357/ac2aa6

Bian, N. H., & Li, G. (2022). Transport of solar energetic particles along stochastic Parker spirals. *The Astrophysical Journal*, *924*(2), 120. https://doi.org/10.3847/1538-4357/ac2fab

Cairns, I. H., Lobzin, V. V., Donea, A., Tingay, S. J., McCauley, P. I., Oberoi, D., et al. (2018). Low altitude solar magnetic reconnection, type III solar radio bursts, and X-ray emissions. *Scientific Reports*, *8*(1), 1676. https://doi.org/10.1038/s41598-018-19195-3

Cane, H. V. (2003). Near-relativistic solar electrons and type III radio bursts. *The Astrophysical Journal*, *598*(2), 1403–1408. https://doi.org/10.1086/379007

Carmichael, H. (1964). In physics of solar flares (451 pp.).

Dröge, W., Kartavykh, Y. Y., Wang, L., Telloni, D., & Bruno, R. (2018). Transport modeling of interplanetary electrons in the 2002 October 20 solar particle event. *The Astrophysical Journal*, *869*(2), 168. https://doi.org/10.3847/1538-4357/aaec6c

Guo, L., Li, G., Reeves, K., & Raymond, J. (2017). Solar flare termination shock and synthetic emission line profiles of the Fe XXI 1354.08 Å line. *The Astrophysical Journal*, *846*(1), L12. https://doi.org/10.3847/2041-8213/aa866a

Haggerty, D. K., & Roelof, E. C. (2002). Impulsive near-relativistic solar electron events: Delayed injection with respect to solar electromagnetic emission. *The Astrophysical Journal*, *579*(2), 841–853. https://doi.org/10.1086/342870

Haggerty, D. K., Roelof, E. C., & Simnett, G. M. (2003). Escaping near-relativistic electron beams from the solar corona. *Advances in Space Research*, *32*(12), 2673–2678. https://doi.org/10.1016/S0273-1177(03)00929-3

Heyvaerts, J., Priest, E. R., & Rust, D. M. (1977). An emerging flux model for the solar phenomenon. *The Astrophysical Journal*, *216*, 123–137. https://doi.org/10.1086/155453

Hirayama, T. (1974). Theoretical model of flares and prominences. I: Evaporating flare model. *Solar Physics*, *34*(2), 323–338. https://doi.org/10.1007/BF00153671

Jokipii, J. R. (1966). Cosmic-ray propagation. I. Charged particles in a random magnetic field. *The Astrophysical Journal*, *146*, 480. https://doi.org/10.1086/148912

Klein, K.-L., Krucker, S., Trottet, G., & Hoang, S. (2005). Coronal phenomena at the release of solar energetic electron events. *Astronomy & Astrophysics*, *431*(3), 1047–1060. https://doi.org/10.1051/0004-6361:20041258

Kopp, R. A., & Pneuman, G. W. (1976). Magnetic reconnection in the corona and the loop prominence phenomenon. *Solar Physics*, *50*(1), 85–98. https://doi.org/10.1007/BF00206193

Krucker, S., Kontar, E. P., Christe, S., & Lin, R. P. (2007). Solar flare electron spectra at the Sun and near the Earth. *The Astrophysical Journal*, *663*(2), L109–L112. https://doi.org/10.1086/519373

Krucker, S., Larson, D. E., Lin, R. P., & Thompson, B. J. (1999). On the origin of impulsive electron events observed at 1 AU. *The Astrophysical Journal*, *519*(2), 864–875. https://doi.org/10.1086/307415

Laitinen, T., Huttunen-Heikinmaa, K., Valtonen, E., & Dalla, S. (2015). Correcting for interplanetary scattering in velocity dispersion analysis of solar energetic particles. *The Astrophysical Journal*, *806*(1), 114. https://doi.org/10.1088/0004-637X/806/1/114

Li, G., Kong, X., Zank, G., & Chen, Y. (2013). On the spectral hardening at ≳300 keV in solar flares. *The Astrophysical Journal*, *769*(1), 22. https://doi.org/10.1088/0004-637X/769/1/22

Li, G., Wu, X., Effenberger, F., Zhao, L., Lesage, S., Bian, N., & Wang, L. (2021). Constraints on the electron acceleration process in solar flare: A case study. *Geophysical Research Letters*, *48*, e2021GL095138. https://doi.org/10.1029/2021GL095138

Li, G., Wu, X., Zhao, L., & Yao, S. (2020). Observations of outward-propagating and mirroring of the same energetic electrons by wind. *The Astrophysical Journal Letters*, *905*(1), L1. https://doi.org/10.3847/2041-8213/abca87

Li, G., Zhao, L., Wang, L., Liu, W., & Wu, X. (2020). Identification of two distinct electron populations in an impulsive solar energetic electron event. *The Astrophysical Journal*, *900*(2), L16. https://doi.org/10.3847/2041-8213/abb098

Li, X., Guo, F., Li, H., & Li, G. (2017). Particle acceleration during magnetic reconnection in a low-beta plasma. *The Astrophysical Journal*, *843*(1), 21. https://doi.org/10.3847/1538-4357/aa745e

Li, Y., Xue, J. C., Ding, M. D., Cheng, X., Su, Y., Feng, L., et al. (2018). Spectroscopic observations of a current sheet in a solar flare. *The Astrophysical Journal*, *853*(1), L15. https://doi.org/10.3847/2041-8213/aaa6c0

Lin, R. P. (1974). Non-relativistic solar electrons. *Space Science Reviews*, *16*, 189.

Lin, R. P. (1985). Energetic solar electrons in the interplanetary medium. *Solar Physics*, *100*(1–2), 537–561. https://doi.org/10.1007/bf00158444

Lin, R. P., Anderson, K. A., Ashford, S., Carlson, C., Curtis, D., Ergun, R., et al. (1995). A three-dimensional plasma and energetic particle investigation for the WIND spacecraft. *Space Science Reviews*, *71*(1), 125–153. https://doi.org/10.1007/BF00751328

Lintunen, J., & Vainio, R. (2004). Solar energetic particle event onset as analyzed from simulated data. *Astronomy & Astrophysics*, *420*(1), 343–350. https://doi.org/10.1051/0004-6361:20034247

Liu, W., Chen, Q., & Petrosian, V. (2013). Plasmoid ejections and loop contractions in an eruptive M7.7 solar flare: Evidence of particle acceleration and heating in magnetic reconnection outflows. *The Astrophysical Journal*, *767*(2), 168. https://doi.org/10.1088/0004-637X/767/2/168

Masson, S., Antiochos, S. K., & DeVore, C. R. (2013). A model for the escape of solar-flare-accelerated particles. *The Astrophysical Journal*, *771*(2), 82. https://doi.org/10.1088/0004-637X/771/2/82

Meegan, C., Lichti, G., Bhat, P. N., Bissaldi, E., Briggs, M. S., Connaughton, V., et al. (2009). The Fermi gamma-ray burst monitor. *The Astrophysical Journal*, *702*(1), 791–804. https://doi.org/10.1088/0004-637X/702/1/791

Mitchell, J. G., de Nolfo, G. A., Hill, M. E., Christian, E. R., McComas, D. J., Schwadron, N. A., et al. (2020). Small electron events observed by Parker solar probe/IS⊙IS during encounter 2. *The Astrophysical Journal*, *902*(1), 20. https://doi.org/10.3847/1538-4357/abb2a4

Moradi, A., & Li, G. (2019). Propagation of scatter-free solar energetic electrons in a meandering interplanetary magnetic field. *The Astrophysical Journal*, *887*(1), 102. https://doi.org/10.3847/1538-4357/ab4f68

Savitzky, A., & Golay, M. J. E. (1964). Smoothing and differentiation of data by simplified least squares procedures. *Analytical Chemistry*, *36*(8), 1627–1639. https://doi.org/10.1021/ac60214a047

Sharma, R., Battaglia, M., Luo, Y., Chen, B., & Yu, S. (2020). Radio and X-ray observations of short-lived episodes of electron acceleration in a solar microflare. *The Astrophysical Journal*, *904*(2), 94. https://doi.org/10.3847/1538-4357/abbd96

Simnett, G. M., Roelof, E. C., & Haggerty, D. K. (2002). The acceleration and release of near-relativistic electrons by coronal mass ejections. *The Astrophysical Journal*, *579*(2), 854–862. https://doi.org/10.1086/342871

Smith, D. M., Lin, R. P., Turin, P., Curtis, D. W., Primbsch, J. H., Campbell, R. D., et al. (2003). The RHESSI spectrometer. In R. P. Lin, B. R. Dennis, & A. O. Benz (Eds.), *The Reuven Ramaty High-Energy Solar Spectroscopic Imager (RHESSI)* (pp. 33–60). Springer Netherlands. https://doi.org/10.1007/978-94-017-3452-3_2

Sturrock, P. A. (1966). Model of the high-energy phase of solar flares. *Nature*, *211*(5050), 695–697. https://doi.org/10.1038/211695a0

Tan, L. C., Malandraki, O. E., Reames, D. V., Ng, C. K., Wang, L., & Dorrian, G. (2012). Use of incident and reflected solar particle beams to trace the topology of magnetic clouds. *The Astrophysical Journal*, *750*(2), 146. https://doi.org/10.1088/0004-637X/750/2/146

Tan, L. C., Reames, D. V., Ng, C. K., Saloniemi, O., & Wang, L. (2009). Observational evidence on the presence of an outer reflecting boundary in solar energetic particle events. *The Astrophysical Journal*, *701*(2), 1753–1764. https://doi.org/10.1088/0004-637X/701/2/1753

Tan, L. C., Reames, D. V., Ng, C. K., Shao, X., & Wang, L. (2011). What causes scatter-free transport of non-relativistic solar electrons? *The Astrophysical Journal*, *728*(2), 133. https://doi.org/10.1088/0004-637X/728/2/133

Vech, D., Mallet, A., Klein, K. G., & Kasper, J. C. (2018). Magnetic reconnection may control the ion-scale spectral break of solar wind turbulence. *The Astrophysical Journal*, *855*(2), L27. https://doi.org/10.3847/2041-8213/aab351

Vršnak, B., Warmuth, A., Maričić, D., Otruba, W., & Ruždjak, V. (2003). Interaction of an erupting filament with the ambient magnetoplasma and escape of electron beams. *Solar Physics*, *217*(1), 187–198. https://doi.org/10.1023/A:1027388929859

Wang, L., Krucker, S., Mason, G. M., Lin, R. P., & Li, G. (2016). The injection of ten electron/$^3$He-rich SEP events. *Astronomy & Astrophysics*, *585*, A119. https://doi.org/10.1051/0004-6361/201527270

Wang, L., Lin, R. P., & Krucker, S. (2011). Pitch-angle distributions and temporal variations of 0.3–300 keV solar impulsive electron events. *The Astrophysical Journal*, *727*(2), 121. https://doi.org/10.1088/0004-637X/727/2/121

Wang, L., Lin, R. P., Krucker, S., & Gosling, J. T. (2006). Evidence for double injections in scatter-free solar impulsive electron events. *Geophysical Research Letters*, *33*, L03106. https://doi.org/10.1029/2005GL024434

Wang, L., Lin, R. P., Krucker, S., & Mason, G. M. (2012). A statistical study of solar electron events over one solar cycle. *The Astrophysical Journal*, *759*(1), 69. https://doi.org/10.1088/0004-637X/759/1/69

Wang, W., Wang, L., Krucker, S., Mason, G. M., Su, Y., & Bučík, R. (2021). Solar energetic electron events associated with hard X-ray flares. *The Astrophysical Journal*, *913*(2), 89. https://doi.org/10.3847/1538-4357/abefce

Williams, P. E., & Pesnell, W. D. (2011). Properties of supergranulation during the solar minima of cycles 22/23 and 23/24. *Journal of Physics: Conference Series*, *271*(1), 012082. https://doi.org/10.1088/1742-6596/271/1/012082

Zhao, L., Li, G., Zhang, M., Wang, L., Moradi, A., & Effenberger, F. (2019). Statistical analysis of interplanetary magnetic field path lengths from solar energetic electron events observed by WIND. *The Astrophysical Journal*, *878*(2), 107. https://doi.org/10.3847/1538-4357/ab2041